Published for SISSA by Springer

Received: March 13, 2021
Revised: June 28, 2021
Accepted: July 29, 2021
Published: August 16, 2021

Axion/hidden-photon dark matter conversion into condensed matter axion

So Chigusa,[a,b,c] **Takeo Moroi**[d,e] **and Kazunori Nakayama**[d,e]

[a] *Berkeley Center for Theoretical Physics, Department of Physics, University of California, South Hall Rd, Berkeley, CA 94720, U.S.A.*

[b] *Theoretical Physics Group, Lawrence Berkeley National Laboratory, 1 Cyclotron Rd, Berkeley, CA 94720, U.S.A.*

[c] *KEK Theory Center, IPNS, KEK, 1-1 Oho, Tsukuba, Ibaraki 305-0801, Japan*

[d] *Department of Physics, Faculty of Science, The University of Tokyo, 7-3-1 Hongo, Bunkyo-ku, Tokyo 113-0033, Japan*

[e] *Kavli IPMU (WPI), The University of Tokyo, 5-1-5 Kashiwanoha, Kashiwa, Chiba 277-8583, Japan*

E-mail: so.chigusa.pp@gmail.com, moroi@phys.s.u-tokyo.ac.jp, kazunori@hep-th.phys.s.u-tokyo.ac.jp

Abstract: The QCD axion or axion-like particles are candidates of dark matter of the universe. On the other hand, axion-like excitations exist in certain condensed matter systems, which implies that there can be interactions of dark matter particles with condensed matter axions. We discuss the relationship between the condensed matter axion and a collective spin-wave excitation in an anti-ferromagnetic insulator at the quantum level. The conversion rate of the light dark matter, such as the elementary particle axion or hidden photon, into the condensed matter axion is estimated for the discovery of the dark matter signals.

Keywords: Cosmology of Theories beyond the SM, Topological States of Matter

ArXiv ePrint: 2102.06179

https://doi.org/10.1007/JHEP08(2021)074

JHEP08(2021)074

Contents

JHEP08(2021)074

1 Introduction

The QCD axion is a hypothetical elementary particle that solves the strong CP problem [1–3] and is a candidate of dark matter (DM) of the universe [4–6] (see refs. [7–9] for reviews). Recently people often consider axion-like particles (ALPs) in a broad sense, partly motivated by the developments in string theory [10–12]. ALPs do not necessarily address the strong CP problem, but they are also good DM candidates and may be experimentally probed through, e.g., the axion-photon coupling of the form $\mathcal{L} \propto a\vec{E}\cdot\vec{B}$ where a denotes the ALP field and $\vec{E}$ ($\vec{B}$) denotes the electric (magnetic) field respectively. There are many

experimental ideas to search for ALPs including the QCD axion,[1] although still it is not discovered yet [13–39].

On the other hand, the axion-like excitation also appears in the condensed matter physics [40, 41] (see refs. [42, 43] for reviews). To distinguish it from the elementary particle axion or ALP, we call such an axion-like excitation in condensed matter context as "condensed matter axion (CM axion)". The CM axion $\delta\theta$ has an interaction with the electromagnetic field as $\mathcal{L} \propto \delta\theta \vec{E} \cdot \vec{B}$, similar to the ALP. We call such an insulator an axionic insulator.

Let us briefly mention a relation between the topological insulator and axionic insulator. In general, topological electromagnetic responses of a three-dimensional insulator are described by the topological term in the Lagrangian:

$$\mathcal{L} = \theta \frac{\alpha_e}{4\pi} F_{\mu\nu} \widetilde{F}^{\mu\nu} = \theta \frac{\alpha_e}{\pi} \vec{E} \cdot \vec{B}. \tag{1.1}$$

For example, it implies that there appears a magnetization (electric polarization) proportional to the applied electric (magnetic) field: $\vec{M} \propto \theta \vec{E}$ ($\vec{P} \propto \theta \vec{B}$). If the Hamiltonian of the system is invariant under the time-reversal symmetry, the coefficient θ can only take a value either 0 or π: i.e., such an insulator is classified by a discrete Z_2 index [44–49].[2] The case of $\theta = \pi$ corresponds to the topological insulator, in which the existence of gapless surface states is ensured and it causes topological electromagnetic effects. On the other hand, if there is no time-reversal symmetry, θ does not have to be quantized but can take arbitrary values possibly with a space-time dependence: $\theta = \theta(\vec{x}, t)$. If θ is a dynamical field, it is called the CM axion. Although it is often helpful to start from the topological insulator for understanding the origin of CM axion, the existence of CM axion does not necessarily require that the insulator is topological. One can generally write $\theta(\vec{x}, t) = \theta_0 + \delta\theta(\vec{x}, t)$ so that $\delta\theta(\vec{x}, t)$ expresses the CM axion while θ_0 is the background value. The value of θ_0 depends on the properties of the material and can be zero. It has been known that in a class of magnetically doped topological insulators, the fluctuation of the anti-ferromagnetic order parameter (the so-called Neel field) plays a role of CM axion [41].

In this paper, we consider a process like the light DM conversion into the CM axion and estimate the conversion rate. Such a process has been considered in ref. [39] for the detection of axion-like DM. One of the main purposes of this paper is to discuss the origin of CM axion in a comprehensive and self-consistent manner for particle physicists. We will explicitly show the relationship between the CM axion and the spin-wave fluctuation (magnon) based on a model presented in ref. [52]. Another purpose is to provide a useful method to calculate the DM conversion rate into the CM axion in a quantum mechanical way. As an illustration, we will consider the case of ALP DM and hidden-photon DM.

This paper is organized as follows. In section 2 we review the (anti-ferromagnetic) Heisenberg model of the localized electron spin system on the lattice. It gives a basis of the collective spin-wave excitation (magnon) and its dispersion relation, which will turn

[1] In the following we use the terminology "ALP" for general elementary axion-like particles including the QCD axion.

[2] Time-reversal invariant topological insulators have been first considered in two-dimensional systems [50, 51].

JHEP08(2021)074

out to be identified with the CM axion in a certain setup. In section 3 the so-called (half-filling) Hubbard model is briefly introduced. Electrons in solids are often modeled by a tight-binding Hamiltonian plus the Coulomb repulsive force between electrons on the same lattice point (Hubbard interaction). It is shown that the limit of large Hubbard interaction reduces to the (anti-ferromagnetic) Heisenberg model. Therefore, the Hubbard model on a certain lattice may describe both the electron energy band structure as well as the anti-ferromagnetic order and magnon excitation around it. In section 4 we introduce the Fu-Kane-Mele-Hubbard model as a concrete setup and show that it contains an excitation that is regarded as the CM axion along the line of ref. [52]. It will become clear that the CM axion is described by the use of anti-ferromagnetic magnon and its dispersion can be estimated as explained in section 2. In section 5 we estimate the conversion rate of light bosonic DM into the CM axion. We consider two DM models: ALP and hidden photon. We conclude in section 6.

2 Magnon in anti-ferromagnet

Let us start with the Heisenberg anti-ferromagnet model [53–55].[3] Suppose a bipartite lattice consisting of sublattices A and B, and on each lattice point $\ell \in$ A or $\ell' \in$ B there is an electron spin $\vec{S}$. Applying an external magnetic field B_0 along the z direction, the model Hamiltonian is given by

$$H = -J \sum_{\langle \ell, \ell' \rangle} \vec{S}_\ell \cdot \vec{S}_{\ell'} - g\mu_B (B_A + B_0) \sum_{\ell \in A} S^z_\ell + g\mu_B (B_A - B_0) \sum_{\ell' \in B} S^z_{\ell'}, \tag{2.1}$$

where $J < 0$ is the exchange interaction, $g = 2$ and $\mu_B = e/(2m_e)$ is the Bohr magneton, and B_A is the anisotropy field. The collective excitation of the spin-wave around the ground state, called magnon, is analyzed through the Holstein-Primakoff transformation,

$$S^+_\ell = \sqrt{2s - a^\dagger_\ell a_\ell}\, a_\ell, \qquad S^-_\ell = a^\dagger_\ell \sqrt{2s - a^\dagger_\ell a_\ell}, \qquad S^z_\ell = s - a^\dagger_\ell a_\ell, \tag{2.2}$$

$$S^+_{\ell'} = b^\dagger_{\ell'} \sqrt{2s - b^\dagger_{\ell'} b_{\ell'}}, \qquad S^-_{\ell'} = \sqrt{2s - b^\dagger_{\ell'} b_{\ell'}}\, b_{\ell'}, \qquad S^z_{\ell'} = -s + b^\dagger_{\ell'} b_{\ell'}, \tag{2.3}$$

where we have defined $S^\pm_\ell = S^x_\ell \pm i S^y_\ell$ and $S^\pm_{\ell'} = S^x_{\ell'} \pm i S^y_{\ell'}$, and the creation-annihilation operators satisfy the commutation relation

$$\left[a_\ell, a^\dagger_m\right] = \delta_{\ell m}, \qquad \left[b_{\ell'}, b^\dagger_{m'}\right] = \delta_{\ell' m'}. \tag{2.4}$$

In addition, s is the spin quantum number; the eigenvalue of $\vec{S}_\ell \cdot \vec{S}_\ell$ is given by $s(s+1)$. The Hamiltonian is rewritten in terms of the creation-annihilation operators as

$$\begin{aligned} H =& 2Nzs^2 J - 2Ns\omega_A - Js \sum_{\langle \ell, \ell' \rangle} \left(a^\dagger_\ell a_\ell + b^\dagger_{\ell'} b_{\ell'} + a^\dagger_\ell b^\dagger_{\ell'} + a_\ell b_{\ell'} \right) \\ &+ (\omega_A + \omega_L) \sum_\ell a^\dagger_\ell a_\ell + (\omega_A - \omega_L) \sum_{\ell'} b^\dagger_{\ell'} b_{\ell'}, \end{aligned} \tag{2.5}$$

[3] As explained in section 3, the Heisenberg anti-ferromagnet model may be understood from the Hubbard model in the limit of strong electron self-interaction at each site.

JHEP08(2021)074

where N is the total number of sites in a sublattice, z denotes the number of adjacent lattice points (e.g. $z = 6$ for simple bipartite cubic lattice), and

$$\omega_L \equiv g\mu_B B_0, \qquad \omega_A \equiv g\mu_B B_A. \tag{2.6}$$

Now let us move to the Fourier space. We define the Fourier component as

$$a_\ell = \frac{1}{\sqrt{N}} \sum_{\vec{k}} e^{-i\vec{k}\cdot\vec{x}_\ell} a_{\vec{k}}, \qquad b_{\ell'} = \frac{1}{\sqrt{N}} \sum_{\vec{k}} e^{i\vec{k}\cdot\vec{x}_{\ell'}} b_{\vec{k}}. \tag{2.7}$$

Substituting this into the Hamiltonian, we find

$$H = \sum_{\vec{k}} \left[(\omega_J + \omega_A + \omega_L) a^\dagger_{\vec{k}} a_{\vec{k}} + (\omega_J + \omega_A - \omega_L) b^\dagger_{\vec{k}} b_{\vec{k}} + \omega_J \gamma_{\vec{k}} (a_{\vec{k}} b_{\vec{k}} + a^\dagger_{\vec{k}} b^\dagger_{\vec{k}}) \right], \tag{2.8}$$

where $\omega_J \equiv -2zsJ$ and

$$\gamma_{\vec{k}} = \frac{1}{z} \sum_{\vec{\delta}} e^{i\vec{k}\cdot\vec{\delta}}, \tag{2.9}$$

with $\vec{\delta}$ being the vector connecting the adjacent lattice points. Finally, it is diagonalized through the Bogoliubov transformation:

$$\alpha_{\vec{k}} = u_{\vec{k}} a_{\vec{k}} - v_{\vec{k}} b^\dagger_{\vec{k}}, \qquad \beta^\dagger_{\vec{k}} = u_{\vec{k}} b^\dagger_{\vec{k}} - v_{\vec{k}} a_{\vec{k}}. \tag{2.10}$$

One can check that the canonical commutation relation is maintained if $|u_{\vec{k}}|^2 - |v_{\vec{k}}|^2 = 1$. The concrete expression is given by

$$|u_{\vec{k}}|^2 = \frac{1}{2} \left(1 + \frac{\omega_J + \omega_A}{\sqrt{(\omega_J + \omega_A)^2 - |\gamma_{\vec{k}}|^2 \omega_J^2}} \right), \quad |v_{\vec{k}}|^2 = \frac{1}{2} \left(-1 + \frac{\omega_J + \omega_A}{\sqrt{(\omega_J + \omega_A)^2 - |\gamma_{\vec{k}}|^2 \omega_J^2}} \right), \tag{2.11}$$

with $\arg(\gamma_{\vec{k}}) = 2\arg(u_{\vec{k}}) = -2\arg(-v_{\vec{k}})$. (Thus, $u_{\vec{k}} v_{\vec{k}}$ is real and negative.) Note that, when $\omega_A \ll \omega_J$, we have large Bogoliubov coefficients $|u_{\vec{k}}|^2 \sim |v_{\vec{k}}|^2 \gg 1$ for $|\vec{k}\cdot\vec{\delta}| \ll 1$. Then, one finds the diagonal Hamiltonian:

$$H = \sum_{\vec{k}} \left[(\omega_{\vec{k}} + \omega_L) \alpha^\dagger_{\vec{k}} \alpha_{\vec{k}} + (\omega_{\vec{k}} - \omega_L) \beta^\dagger_{\vec{k}} \beta_{\vec{k}} \right]. \tag{2.12}$$

Here, $\omega_{\vec{k}}$ represents the magnon dispersion relation (besides the overall offset coming from the Larmor frequency ω_L),

$$\omega^2_{\vec{k}} = \omega_J^2 (1 - |\gamma_{\vec{k}}|^2) + \omega_A(\omega_A + 2\omega_J). \tag{2.13}$$

In the low frequency limit $|\vec{k}\cdot\vec{\delta}| \ll 1$, we obtain $\gamma_{\vec{k}} \simeq 1 + i\sum_{\vec{\delta}}(\vec{k}\cdot\vec{\delta})/z - \sum_{\vec{\delta}}(\vec{k}\cdot\vec{\delta})^2/z$. It implies the linear dispersion relation, $\omega_{\vec{k}} \propto |\vec{k}|$ for large $|\vec{k}|$ (but still it satisfies $|\vec{k}\cdot\vec{\delta}| \ll 1$), in contrast to the ferromagnetic magnon dispersion relation, which would show $\omega_{\vec{k}} \propto k^2$. They are related to the so-called type-I and type-II Nambu-Goldstone boson dispersion relation as generally classified in refs. [56, 57].

JHEP08(2021)074

3 Hubbard model as origin of anti-ferromagnet

3.1 Tight-binding model

A tight-binding model is one of the approaches to estimate the electron energy band structure in solids. In this approach, one starts with the picture that each electron is rather tightly bounded by each atom and then takes into account the overlap between the nearest electron wave function.

Let us consider only one electron orbital at each site and neglect the interaction among different orbits, spin-orbit coupling, electron self-interaction, etc.[4] In the second quantization picture, the tight-binding Hamiltonian is given by

$$H = -t \sum_{\langle i,j\rangle,\sigma} c^\dagger_{i\sigma} c_{j\sigma}, \tag{3.1}$$

where $c^\dagger_{i\sigma}$ and $c_{i\sigma}$ denote the electron creation and annihilation operators at the site i with spin σ ($\uparrow$ or $\downarrow$) and the summation is taken over the combination of adjacent sites $\langle i,j\rangle$. The creation and annihilation operators satisfy the anti-commutation relation

$$\left\{c_{i\sigma}, c^\dagger_{j\sigma'}\right\} = \delta_{ij}\delta_{\sigma\sigma'}. \tag{3.2}$$

The Fourier transformation is defined by

$$c_{i\sigma} = \frac{1}{\sqrt{N}} \sum_{\vec{k}} e^{-i\vec{k}\cdot\vec{x}_i} c_{\vec{k},\sigma}. \tag{3.3}$$

The Hamiltonian is rewritten in a diagonal form as

$$H = \sum_{\vec{k},\sigma} \epsilon_{\vec{k}} c^\dagger_{\vec{k},\sigma} c_{\vec{k},\sigma}, \qquad \epsilon_{\vec{k}} = -t(\gamma_{\vec{k}} + \gamma^*_{\vec{k}}). \tag{3.4}$$

This $\epsilon_{\vec{k}}$ denotes the electron energy band. In a simple cubic lattice, for example, we obtain $\epsilon_k = 2t\left(1 - \sum_{i=x,y,z}\cos(k_i a)\right)$.

The conductivity of this model is determined by the number of electrons in the system. If each orbital is filled, i.e., there are two electrons with opposite spins at each site, the energy band is filled and this becomes an insulator as far as there is an energy gap to the next energy band. If there is only one electron at each orbital, the energy band is not filled and it becomes a metal.

3.2 Half-filling Hubbard model

Let us add the effect of interaction between electrons at the same site i to the tight-binding Hamiltonian. The resulting Hamiltonian is called the Hubbard model:

$$H = H_t + H_U = -t \sum_{\langle i,j\rangle,\sigma} c^\dagger_{i\sigma} c_{j\sigma} + U \sum_i n_{i\uparrow} n_{i\downarrow}, \tag{3.5}$$

where $U > 0$ represents the interaction energy and $n_{i\uparrow} = c^\dagger_{i\uparrow} c_{i\uparrow}$ and $n_{i\downarrow} = c^\dagger_{i\downarrow} c_{i\downarrow}$.

[4] Effects of the interaction among different orbitals and spin-orbit coupling are important for the topological insulator. The electron self-interaction will be taken into account in the next subsection.

JHEP08(2021)074

The Hubbard model is characterized by several parameters: the relative interaction strength U/t and the number of electrons per site, N_e/N_s. The case of $N_e/N_s = 1$ is called the half-filling (it is "half" because of the spin degree of freedom) and its properties are well understood. Below, we consider the half-filling case. Naively, one may consider that the half-filling Hubbard model describes a metal since electrons are in a conducting band. It is true in the limit $U = 0$, but it is not necessarily true for sizable interaction strength. The interaction term can split the energy band and make a gap, which would result in an insulator. Such an insulator is called the Mott insulator.

Now we consider the large interaction limit: $U/t \gg 1$. In this limit, the tight-binding part is regarded as a perturbation. In the ground state, one electron is localized at each site to minimize the Hubbard interaction energy (hence it is expected that it behaves as an insulator rather than metal). Thus, the ground state is expressed as

$$|\widetilde{\sigma}\rangle = \left(\prod_i c^\dagger_{i\sigma_i}\right)|0\rangle\,, \tag{3.6}$$

where $\widetilde{\sigma}$ schematically represents the array of spin, e.g., $\widetilde{\sigma} = (\dots,\uparrow,\uparrow,\downarrow,\dots)$ and so on. There are 2^{N_e} degenerate ground states corresponding to the spin degree of freedom at each site.

We want to consider an effective Hamiltonian regarding H_t as a perturbation. Noting $\langle\widetilde{\sigma}|\,H_t\,|\widetilde{\sigma}\rangle = 0$, the nontrivial effect appears at the second-order in H_t. The effective Hamiltonian is given by

$$H_{\text{eff}} = -\mathcal{P}H_t\frac{1}{H_U}H_t\mathcal{P} = -\frac{t^2}{U}\mathcal{P}\sum_{\langle i,j\rangle\sigma\sigma'}\left(c^\dagger_{i\sigma}c_{j\sigma}c^\dagger_{j\sigma'}c_{i\sigma'} + c^\dagger_{j\sigma}c_{i\sigma}c^\dagger_{i\sigma'}c_{j\sigma'}\right)\mathcal{P}, \tag{3.7}$$

where $\mathcal{P}$ denotes the projection operator to the Hilbert space spanned by the ground state (3.6). The physical meaning is that, for $\sigma \neq \sigma'$, it exchanges the spin at the adjacent sites i and j for a given ground state. This is rewritten in terms of the spin operator as

$$H_{\text{eff}} = \frac{4t^2}{U}\sum_{\langle i,j\rangle}\vec{S}_i\cdot\vec{S}_j, \tag{3.8}$$

where we have defined

$$S^z_i = \frac{1}{2}(c^\dagger_{i\uparrow}c_{i\uparrow} - c^\dagger_{i\downarrow}c_{i\downarrow}), \qquad S^+_i \equiv S^x_i + iS_y = c^\dagger_{i\uparrow}c_{i\downarrow}, \qquad S^-_i \equiv S_x - iS_y = c^\dagger_{i\downarrow}c_{i\uparrow}. \tag{3.9}$$

Since the coefficient t^2/U is positive, it represents the Heisenberg anti-ferromagnet model with $J = -t^2/U$. Thus, the half-filling Hubbard model may describe both the metal phase in the limit $U \to 0$ and the anti-ferromagnetic insulator phase in the large U limit.

4 A model of condensed matter axion

4.1 Energy band in Fu-Kane-Mele-Hubbard model

A three-dimensional topological insulator has been proposed in refs. [45, 46]. An example is the diamond lattice with a strong spin-orbit coupling. On the other hand, taking account

JHEP08(2021)074

of the Hubbard on-site interaction between electrons may lead to the anti-ferromagnetic phase, leading to the topological anti-ferromagnet. Such a model is called the Fu-Kane-Mele-Hubbard model and studied in ref. [52]. Actually, it is found in ref. [52] that there is a topological anti-ferromagnetic phase depending on the interaction strength, in which the spin-wave excitation (magnon) has an axionic coupling to the electromagnetic field. Note that no material is found yet that is described by the Fu-Kane-Mele-Hubbard model despite its theoretical tractability. Materials that are associated with the condensed matter axion modes include the Fe-doped Bismuth Selenide, but the treatment of the axion modes in this material requires a more involved approach than the one described below. However, we only focus on the Fu-Kane-Mele-Hubbard model in this paper to demonstrate the derivation of the DM conversion rate into a condensed matter axion in the simplest possible way.

Now, we briefly review the Fu-Kane-Mele-Hubbard model on the diamond lattice. We assume the half-filling case, i.e., there is only one electron at the electron orbitals of our interest at each site. The model Hamiltonian is given by $H = H_0 + H_U$:

$$H_0 = \sum_{\langle i,j\rangle\sigma} t_{ij} c^\dagger_{i\sigma} c_{j\sigma} + i\frac{4\lambda}{a^2} \sum_{\langle\langle i,j\rangle\rangle} c^\dagger_i \vec{\sigma}\cdot(\vec{d^1_{ij}} \times \vec{d^2_{ij}}) c_j, \tag{4.1}$$

$$H_U = U \sum_i n_{i\uparrow} n_{i\downarrow}, \tag{4.2}$$

where $c_i \equiv (c_{i\uparrow}, c_{i\downarrow})^T$. Here, $\vec{d^1_{ij}}$ and $\vec{d^2_{ij}}$ are the two vectors that connect two adjacent sites: $\frac{a}{4}(1,1,1)$, $\frac{a}{4}(1,-1,-1)$, $\frac{a}{4}(-1,1,-1)$, $\frac{a}{4}(-1,-1,1)$, with a being the lattice constant and λ represents the strength of the spin-orbit coupling. Note that the diamond lattice consists of two sublattices (which we call A and B) both of which are face-centered cubic. $\langle\langle i,j\rangle\rangle$ denotes a set of the next-nearest neighbor sites, and hence sites i and j belong to the same sublattice. (For more detail about the interaction of electrons in next-nearest neighbor sites, see appendix A.)

Let us study the energy bands of this model neglecting the Hubbard interaction term [45, 46]. In the Fourier space, the Hamiltonian is expressed as the matrix form in the basis $c_{\vec{k}} \equiv (c_{\vec{k}\uparrow,A}, c_{\vec{k}\downarrow,A}, c_{\vec{k}\uparrow,B}, c_{\vec{k}\downarrow,B})^T$ as

$$H_0 = \sum_{\vec{k}} c^\dagger_{\vec{k}} \mathcal{H} c_{\vec{k}}, \qquad \mathcal{H} = \sum_{\mu=1}^{5} R_\mu(\vec{k})\alpha_\mu, \tag{4.3}$$

where

$$R_1(\vec{k}) = \lambda\left[\sin(\vec{k}\cdot\vec{a}_2) - \sin(\vec{k}\cdot\vec{a}_3) - \sin(\vec{k}\cdot(\vec{a}_2-\vec{a}_1)) - \sin(\vec{k}\cdot(\vec{a}_3-\vec{a}_1))\right], \tag{4.4}$$

$$R_2(\vec{k}) = \lambda\left[\sin(\vec{k}\cdot\vec{a}_3) - \sin(\vec{k}\cdot\vec{a}_1) - \sin(\vec{k}\cdot(\vec{a}_3-\vec{a}_2)) - \sin(\vec{k}\cdot(\vec{a}_1-\vec{a}_2))\right], \tag{4.5}$$

$$R_3(\vec{k}) = \lambda\left[\sin(\vec{k}\cdot\vec{a}_1) - \sin(\vec{k}\cdot\vec{a}_2) - \sin(\vec{k}\cdot(\vec{a}_1-\vec{a}_3)) - \sin(\vec{k}\cdot(\vec{a}_2-\vec{a}_3))\right], \tag{4.6}$$

$$R_4(\vec{k}) = t\left[1 + \cos(\vec{k}\cdot\vec{a}_1) + \cos(\vec{k}\cdot\vec{a}_2) + \cos(\vec{k}\cdot\vec{a}_3)\right] + \delta t, \tag{4.7}$$

$$R_5(\vec{k}) = t\left[\sin(\vec{k}\cdot\vec{a}_1) + \sin(\vec{k}\cdot\vec{a}_2) + \sin(\vec{k}\cdot\vec{a}_3)\right], \tag{4.8}$$

JHEP08(2021)074

with $\vec{a}_1 = \frac{a}{2}(0,1,1), \vec{a}_2 = \frac{a}{2}(1,0,1), \vec{a}_3 = \frac{a}{2}(1,1,0)$ and

$$\alpha_i = \begin{pmatrix} \sigma_i & 0 \\ 0 & -\sigma_i \end{pmatrix}, \quad \alpha_4 = \begin{pmatrix} 0 & 1 \\ 1 & 0 \end{pmatrix}, \quad \alpha_5 = \begin{pmatrix} 0 & i \\ -i & 0 \end{pmatrix}. \tag{4.9}$$

These α matrices are Hermite and satisfy the anti-commutation relation $\{\alpha_\mu, \alpha_\nu\} = 2\delta_{\mu\nu}$. Then, it is easy to show that the energy eigenvalues are given by

$$E_\pm = \pm\sqrt{\sum_\mu \left(R_\mu(\vec{k})\right)^2}. \tag{4.10}$$

This gives the dispersion relation of the bulk electron. It is found that, at the so-called X_r points ($r = 1, 2, 3$) of the momentum space, $\vec{k}_{X_1} = \frac{2\pi}{a}(1,0,0), \vec{k}_{X_2} = \frac{2\pi}{a}(0,1,0), \vec{k}_{X_3} = \frac{2\pi}{a}(0,0,1)$, which are located at the boundary of the Brillouin zone, we obtain $E_\pm = 0$ in the limit of $\delta t = 0$. Thus, this material is regarded as a semimetal in this limit. For example, the dispersion relation around $\vec{k} = \vec{k}_{X_1}$ is given by

$$E_\pm(\vec{q}) = \pm\sqrt{(tq_x)^2 + 4\lambda^2(q_y^2 + q_z^2) + (\delta t)^2}, \tag{4.11}$$

where we have taken $\vec{k} = \vec{k}_{X_1} + \vec{q}$. Thus, nonzero δt gives the energy gap between two energy bands, which makes the material the bulk insulator (topological insulator, actually).

4.2 Axionic excitation in anti-ferromagnetic phase

It is expected that the inclusion of the Hubbard interaction H_U may lead to the anti-ferromagnetic ordering. Actually, it is found that the anti-ferromagnetic phase appears for sizable U/t in the mean field approximation [52]. Under this approximation, the Hubbard interaction term can be rewritten as

$$\begin{aligned} H_U \simeq U \sum_i \Big(& \langle n_{i\uparrow}\rangle n_{i\downarrow} + \langle n_{i\downarrow}\rangle n_{i\uparrow} - \langle n_{i\uparrow}\rangle \langle n_{i\downarrow}\rangle \\ & - \left\langle c_{i\uparrow}^\dagger c_{i\downarrow}\right\rangle c_{i\downarrow}^\dagger c_{i\uparrow} - \left\langle c_{i\downarrow}^\dagger c_{i\uparrow}\right\rangle c_{i\uparrow}^\dagger c_{i\downarrow} + \left\langle c_{i\uparrow}^\dagger c_{i\downarrow}\right\rangle \left\langle c_{i\downarrow}^\dagger c_{i\uparrow}\right\rangle \Big), \end{aligned} \tag{4.12}$$

with $\langle \mathcal{O} \rangle$ being the ensemble average of the operator $\mathcal{O}$. We use the operator equations

$$n_{i\uparrow(\downarrow)} = \pm S_i'^z + \frac{1}{2}(n_{i\uparrow} + n_{i\downarrow}), \tag{4.13}$$

$$c_{i\uparrow}^\dagger c_{i\downarrow} = S_i'^x + iS_i'^y, \tag{4.14}$$

$$c_{i\downarrow}^\dagger c_{i\uparrow} = S_i'^x - iS_i'^y, \tag{4.15}$$

with $\vec{S}_i'$ being spin operators in the coordinate system used in the previous subsection, with which three Dirac points are defined. Note that, in the $U \to \infty$ limit of a half-filling model, we can safely restrict ourselves to states with $\langle n_{i\uparrow} + n_{i\downarrow}\rangle = 1$. Then, neglecting constant terms, the Hubbard interaction becomes

$$H_U \ni \sum_{\vec{k}} c_{\vec{k}}^\dagger \mathcal{H}_U c_{\vec{k}}, \qquad \mathcal{H}_U = -U \sum_{r=1}^{3} m_r \alpha_r, \tag{4.16}$$

JHEP08(2021)074

with m_r are defined through

$$\left\langle \vec{S}_{i,A} \right\rangle = -\left\langle \vec{S}_{i,B} \right\rangle \equiv \vec{m}, \tag{4.17}$$

which characterizes the anti-ferromagnetic ordering.

Under this background and assuming $U|\vec{m}| \ll \lambda$, the X_r points ($r = 1, 2, 3$) are slightly shifted as

$$\vec{k}_{\widetilde{X}_1} = \left(\frac{2\pi}{a}, \frac{Um_2}{2\lambda a}, -\frac{Um_3}{2\lambda a}\right), \vec{k}_{\widetilde{X}_2} = \left(-\frac{Um_1}{2\lambda a}, \frac{2\pi}{a}, \frac{Um_3}{2\lambda a}\right), \vec{k}_{\widetilde{X}_3} = \left(\frac{Um_1}{2\lambda a}, -\frac{Um_2}{2\lambda a}, \frac{2\pi}{a}\right). \tag{4.18}$$

For example, the energy dispersion around the $\widetilde{X}_1$ point is given by

$$E_{\pm}(\vec{q}) = \pm\sqrt{(tq_x)^2 + 4\lambda^2(q_y^2 + q_z^2) + (\delta t)^2 + (Um_1)^2}, \tag{4.19}$$

where we have taken $\vec{k} = \vec{k}_{\widetilde{X}_1} + \vec{q}$. It is seen that there is an additional gap due to the anti-ferromagnetic order.

The Hamiltonian around the $\widetilde{X}_1$ point is expressed as

$$\mathcal{H}_{\widetilde{X}_1}(\vec{q}) = \widetilde{q}_x\alpha_1 + \widetilde{q}_y\alpha_2 + \widetilde{q}_z\alpha_3 + \delta t\,\alpha_4 + Um_1\alpha_5, \tag{4.20}$$

where we have rescaled the momentum as $tq_x \to \widetilde{q}_x/a$, $2\lambda q_y \to \widetilde{q}_y/a$, $2\lambda q_z \to \widetilde{q}_z/a$. In deriving eq. (4.20), we have performed an appropriate change of the basis of the α matrices through a unitary transformation, with which $\alpha_1 \leftrightarrow \alpha_5$ (see appendix B). The Hamiltonian around the $\widetilde{X}_2$ and $\widetilde{X}_3$ points can also be reduced to the same form except for the last term, which becomes $Um_2\alpha_5$ and $Um_3\alpha_5$, respectively. From this Hamiltonian, we can infer the effective action for the electron which mimics the action of the relativistic Dirac fermion as

$$S = \int d^4x \sum_{r=1,2,3} \overline{\psi}_r \left[i\gamma^\mu(\partial_\mu - ieA_\mu) - \delta t - i\gamma_5 Um_r\right]\psi_r. \tag{4.21}$$

One can make a chiral rotation of the fermion to eliminate the γ_5 dependent term, $\psi_r \to e^{i\gamma_5\theta_r/2}\psi_r$. Then, there appears a topological term:[5]

$$S = \int d^4x\,\theta\frac{\alpha_e}{4\pi}F_{\mu\nu}\widetilde{F}^{\mu\nu}, \qquad \theta \equiv \theta_0 + \sum_r \theta_r = \theta_0 + \sum_r \tan^{-1}\left(\frac{Um_r}{\delta t}\right), \tag{4.22}$$

where θ_0 is either 0 or π depending on the sign of δt. (See appendix C for another derivation of θ.) Note that the background magnetization $\vec{m}$ can fluctuate: it is a spin-wave or magnon excitation, $\vec{m}(\vec{x})$. Then, $\theta(\vec{x})$ is not a constant but a dynamical field and it has an axionic coupling to the electromagnetic field. Therefore, in this model, the magnon effectively behaves as an axion-like field (CM axion).

[5] Eq. (4.22) may not be applicable when $Um_r/\delta t \gg 1$ [52].

JHEP08(2021)074

4.3 Axionic excitation as magnons

To relate the axionic excitation (or the CM axion) θ to the conventional magnons defined in section 2, we repeat the analysis in the previous subsection, taking into account the fluctuation of the background magnetization in terms of magnon operators. We focus only on the spatially homogeneous spin fluctuations and consider their interaction with electrons at around a Dirac point $\vec{k} \sim \vec{k}_{\widetilde{X}_r}$. Then, the relevant part of the Hubbard interaction term is schematically expressed as

$$H_U \ni U \sum_{r=1,2,3} \sum_{\vec{k} \sim \vec{k}_{\widetilde{X}_r}} \sum_{L=A,B} \Big[\widetilde{F}_L(n_{i\uparrow}; \vec{0})(c^\dagger_{\vec{k}\downarrow,L} c_{\vec{k}\downarrow,L}) + \widetilde{F}_L(n_{i\downarrow}; \vec{0})(c^\dagger_{\vec{k}\uparrow,L} c_{\vec{k}\uparrow,L}) \\ - \widetilde{F}_L(c^\dagger_{i\uparrow} c_{i\downarrow}; \vec{0})(c^\dagger_{\vec{k}\downarrow,L} c_{\vec{k}\uparrow,L}) - \widetilde{F}_L(c^\dagger_{i\downarrow} c_{i\uparrow}; \vec{0})(c^\dagger_{\vec{k}\uparrow,L} c_{\vec{k}\downarrow,L}) \Big], \quad (4.23)$$

where the Fourier transform of operators $\mathcal{O}_i$ is defined as

$$\widetilde{F}_L(\mathcal{O}_i; \vec{q}) \equiv \frac{1}{N} \sum_{i \in L} \mathcal{O}_i e^{i\vec{q}\cdot\vec{x}_i}. \quad (4.24)$$

$\tilde{F}_L$ in eq. (4.23) is determined by the magnetization, which may fluctuate around the average value. We again use the operator equations eqs. (4.13)–(4.15) to rewrite $\tilde{F}_L$ in terms of spin operators $\vec{S}'_i$. The relationship between $\vec{S}'_i$ and $\vec{S}_i$, which are defined in section 2 and directly related to magnon operators, is given by

$$\vec{S}'^{A(B)}_i = O \vec{S}^{A(B)}_i, \quad (4.25)$$

with $O \equiv (\vec{o}_1\ \vec{o}_2\ \vec{o}_3)$ being a 3×3 rotation matrix with $\vec{m} \parallel \vec{o}_3$.[6]

Taking everything into consideration, the magnon-Dirac electron interaction term is, up to some constant and quadratic terms of magnons, expressed as

$$H_U \ni \sum_{\vec{k}} c^\dagger_{\vec{k}} \widetilde{\mathcal{H}}_U c_{\vec{k}}, \qquad \widetilde{\mathcal{H}}_U = \sum_{\mu=1}^{5} \widetilde{R}_\mu \alpha_\mu + \widetilde{R}_{12}\alpha_{12} + \widetilde{R}_{23}\alpha_{23} + \widetilde{R}_{31}\alpha_{31}, \quad (4.26)$$

with $\alpha_{rr'} \equiv -i\alpha_r\alpha_{r'}$. Coefficients are given by

$$\widetilde{R}_r = -U \left[m_r + \sqrt{\frac{s}{8N}} \left((O_{r1} - iO_{r2})(u_{\vec{0}} - v_{\vec{0}})(\alpha_{\vec{0}} - \beta^\dagger_{\vec{0}}) + \text{h.c.} \right) \right] \quad (r = 1, 2, 3), \quad (4.27)$$

$$\widetilde{R}_4 = \widetilde{R}_5 = 0, \quad (4.28)$$

where $O_{rr'}$ is the (r, r') component of the rotation matrix O, while $m_r \equiv O_{r3}(s - \frac{1}{N}\sum_{\vec{q}} v_{\vec{q}})$ is the r-th component of the sublattice magnetization in the ground state. In addition, here and hereafter, $s = 1/2$. Bogoliubov coefficients $u_{\vec{0}}$ and $v_{\vec{0}}$ to define the magnon mass basis, i.e., α- and β-modes, are given by eq. (2.11). Since the magnon mass basis is a nontrivial mixture of the original basis, the ground state includes non-zero occupation

[6] There is an ambiguity in the choice of $\vec{o}_1$ and $\vec{o}_2$ related to the $SO(2)$ rotation around $\vec{o}_3$. However, since (4.29) is unchanged under the $SO(2)$ up to an overall phase factor, it does not affect the interaction strength.

JHEP08(2021)074

number in terms of the original basis and $|v_{\vec{0}}|^2$ roughly measures it. Recalling that they satisfy $|u_{\vec{0}}|^2 - |v_{\vec{0}}|^2 = 1$, the small mixing limit corresponds to $u_{\vec{0}} - v_{\vec{0}} \simeq 1$. Note that the expectation value of $\widetilde{R}_r$ is proportional to the r-th component of the order parameter $(\langle S_{i,A}\rangle - \langle S_{i,B}\rangle)/2$, while that of $\widetilde{R}_{rr'}$ to the average magnetization $(\langle S_{i,A}\rangle + \langle S_{i,B}\rangle)/2$. The $\widetilde{R}_{rr'}$ terms induce interactions between magnon and electron/hole. It may cause, for example, the decay of a magnon into an electron-hole pair when the gap is small. Because we are interested in the magnon interaction with electromagnetic fields, which is not induced by the $\widetilde{R}_{rr'}$ terms, we neglect them from now on. Repeating the same procedure as section 4.2, we obtain the relationship between the axionic excitation and magnons. Finally, the electromagnetic interaction of magnons is described by

$$H_{\rm int} = -\frac{\alpha_e}{4\pi}\sqrt{\frac{s}{2N}}(u_{\vec{0}} - v_{\vec{0}})\left[D^*\alpha^\dagger_{\vec{0}} - D\beta^\dagger_{\vec{0}} + \text{h.c.}\right]\int d^3x\, \vec{E}\cdot\vec{B}, \tag{4.29}$$

with

$$D = \sum_r \frac{U/\delta t}{1 + U^2 m_r^2/\delta t^2}(O_{r1} - iO_{r2}), \tag{4.30}$$

being an $O(1)$ factor, assuming only a moderate hierarchy between U and δt. Note that $(u_{\vec{0}} - v_{\vec{0}})$ is real because $\gamma_{\vec{0}} = 1$. The interaction Hamiltonian shows that a linear combination of magnon states is excited by a non-zero value of $\vec{E}\cdot\vec{B}$.

One may embed the CM axions into canonically normalized scalar fields, which we denote $a^{(\alpha)}_{\rm CM}$ and $a^{(\beta)}_{\rm CM}$ for α- and β-modes, respectively. Then, the effective interaction Hamiltonian of these CM axion fields can be written as

$$H_{\rm int} = \frac{\alpha_e}{\sqrt{2}\pi f_{\rm CM}}\int d^3x \left(a^{(\alpha)}_{\rm CM} + a^{(\beta)}_{\rm CM}\right)\vec{E}\cdot\vec{B},$$

where $f_{\rm CM}$ is the "decay constant" of the CM axion. Using eq. (4.29), the decay constant is found to be $f_{\rm CM} = 2\sqrt{2}/[(u_{\vec{0}} - v_{\vec{0}})|D|\sqrt{s\omega_{\vec{0}}V_{\rm unit}}]$ with $\omega_{\vec{0}}$ being the magnon frequency at $\vec{k} = \vec{0}$ and $V_{\rm unit} = V/N$ the volume of the magnetic unit cell. The reference scale is $f_{\rm CM} \simeq 1\,\text{MeV}$ for $\omega_{\vec{0}} = 1\,\text{meV}$, $V_{\rm unit} = (0.3\,\text{keV})^{-3}$ and $(u_{\vec{0}} - v_{\vec{0}})|D| = 1$.

5 Dark matter conversion into condensed matter axion

Now we discuss the detection of the elementary-particle DM axion (or ALPs) and hidden photon through the interaction with CM axion. (To avoid confusion between the DM and CM axions, hereafter, the DM axion and ALPs are both called ALPs.)

5.1 ALP dark matter

The dynamics of the ALP DM a and the photon in a material is described by

$$\mathcal{L} = \frac{1}{2}(\partial_\mu a)^2 - \frac{m_a^2}{2}a^2 + \frac{1}{2}\left(\epsilon|\vec{E}|^2 - \frac{|\vec{B}|^2}{\mu}\right) + g_{a\gamma\gamma}a\vec{E}\cdot\vec{B}, \tag{5.1}$$

JHEP08(2021)074

where ϵ and μ are the permittivity and permeability of the material. Hereafter, we treat the ALP field as a classical background

$$a(\vec{x},t) = a_0 \cos(m_a t - m_a \vec{v}_a \cdot \vec{x} + \delta), \tag{5.2}$$

with $|\vec{v}_a| \sim O(10^{-3})$. When the ALP explains the total amount of the dark matter $\rho_{\rm DM} \sim 0.3\,{\rm GeV/cm^3}$, we obtain $m_a^2 a_0^2/2 = \rho_{\rm DM}$. We consider applying a constant magnetic field $\vec{B}_0 = B_0 \hat{z}$ to the system, where $\hat{z}$ is a unit vector along the z-axis. This magnetic field, combined with the ALP background, generates an oscillating electric field

$$\vec{E}(\vec{x},t) = E_0 \hat{z} \cos(m_a t - m_a \vec{v}_a \cdot \vec{x} + \delta), \tag{5.3}$$

with

$$E_0 = -\frac{1}{\epsilon} g_{a\gamma\gamma} a_0 B_0. \tag{5.4}$$

The target mass range of this set up is $m_a \sim O(10^{-3})\,{\rm eV}$, which has a de-Broglie length $\ell \sim 1/m_a|\vec{v}_a| \sim O(10)\,{\rm cm}$. We assume that ℓ is larger than the material size and neglect the $\vec{x}$ dependence of the ALP background inside the material. Since $\vec{E}\cdot\vec{B}$ is uniform in this case, only the magnon zero-modes may be excited, which are considered in section 4.3. Substituting the value of $\vec{E}\cdot\vec{B}$ generated by the ALP background, the interaction Hamiltonian is rewritten as

$$H_{\rm int} = (C_a^* \alpha_{\vec{0}}^\dagger - C_a \beta_{\vec{0}}^\dagger + {\rm h.c.}) \cos(m_a t + \delta), \tag{5.5}$$

where

$$C_a \equiv -\frac{\alpha_e E_0 B_0 V}{4\pi} \sqrt{\frac{s}{2N}} (u_{\vec{0}} - v_{\vec{0}}) D, \tag{5.6}$$

with V being the material volume. $H_{\rm int}$ describes the generation of both α- and β-modes of the magnon. However, as we will see below, one of them is highly enhanced when the corresponding excitation energy matches with the ALP mass; in such a case, we may expect an observable signal rate at the laboratory. Accordingly, we will estimate a signal rate of the magnon excitation assuming that a single mode is selectively excited.[7]

We start from the α-mode, while the discussion for the β-mode is parallel, as we will comment later. We define the ground and the one-magnon states of the material through $\alpha_{\vec{q}}|0\rangle = \beta_{\vec{q}}|0\rangle = 0$ for any $\vec{q}$ and $|1\rangle \equiv \alpha_{\vec{0}}^\dagger |0\rangle$, respectively. Also, we express the state of the material at the time t as[8]

$$|\psi(t)\rangle \equiv a_0(t)\,|0\rangle + a_1(t)\,|1\rangle\,, \tag{5.7}$$

[7] Precisely speaking, the α- and β-modes are not mass eigenstates since they mix with a photon, forming the so-called axionic polariton [41]. However, since the mixing is expected to be small for a small momentum, we neglect it in our analysis.

[8] The occupation number can be larger than 1. In the present case, however, the expectation value of the occupation number is much smaller than 1, and the states with higher occupation numbers are irrelevant.

JHEP08(2021)074

and consider its time evolution described by

$$i\frac{\partial}{\partial t}\left|\psi(t)\right\rangle = (H + H_{\rm int})\left|\psi(t)\right\rangle, \tag{5.8}$$

where H and $H_{\rm int}$ are given in eqs. (2.12) and (5.5), respectively. We treat $H_{\rm int}$ as a perturbation and evaluate the time evolution perturbatively. Expressing the time derivative with a dot, the evolution of coefficients $a_0(t)$ and $a_1(t)$ is described as

$$i\dot{a}_0 = C_a^* \cos(m_a t + \delta) a_1, \tag{5.9}$$

$$i\dot{a}_1 = m_m a_1 + C_a \cos(m_a t + \delta) a_0, \tag{5.10}$$

where the magnon mass is defined as $m_m \equiv \omega_{\vec{0}} + \omega_L$. By solving these equations, we obtain

$$a_1(t) \simeq -\frac{C_a}{2}\frac{e^{i\delta}(m_a - m_m)(e^{im_a t} - e^{-im_m t}) - e^{-i\delta}(m_a + m_m)(e^{-im_a t} - e^{-im_m t})}{m_a^2 - m_m^2}. \tag{5.11}$$

The probability that we find a one-magnon state $|1\rangle$ at the time t is given by $P(t) \equiv |a_1(t)|^2$. $P(t)$ is highly enhanced when $m_m \simeq m_a$, with which we obtain

$$P(t) \simeq \frac{|C_a|^2 t^2}{4}. \tag{5.12}$$

For the β-mode, we can repeat the discussion by defining $|1\rangle \equiv \beta_{\vec{0}}^\dagger |0\rangle$, and all the calculations are the same but replacements $C_a \to C_a^*$ and $\omega_L \to -\omega_L$.

$P(t)$ can not become infinitely large because there is an upper limit on t for several reasons; one of them is the ALP coherence time $\tau_a \sim 1/m_a v_a^2$ and another is the magnon dissipation time τ_m. Neglecting other possible sources of limitation for simplicity, we define the effective coherence time $\tau \equiv \min(\tau_a, \tau_m)$. Then, the average magnon excitation rate is evaluated as

$$\frac{dN_{\rm signal}}{dt} = \frac{P(\tau)}{\tau} = \frac{|C_a|^2 \tau}{4}. \tag{5.13}$$

Numerically, the signal rate is evaluated as

$$\begin{aligned}\frac{dN_{\rm signal}}{dt} \sim 0.002\,{\rm s}^{-1} &\left(\frac{B_0}{1\,{\rm T}}\right)^4 (u_{\vec{0}} - v_{\vec{0}})^2 \left(\frac{V_{\rm unit}}{(0.3\,{\rm keV})^{-3}}\right)\left(\frac{V}{(10\,{\rm cm})^3}\right) \\ &\times \frac{|D|^2}{\epsilon^2}\left(\frac{g_{a\gamma\gamma}}{10^{-10}\,{\rm GeV}^{-1}}\right)^2 \left(\frac{10^{-3}\,{\rm eV}}{m_a}\right)^2 \left(\frac{\tau}{0.1\,\mu{\rm s}}\right),\end{aligned} \tag{5.14}$$

where $V/N = V_{\rm unit}$ with $V_{\rm unit}$ being the volume of the magnetic unit cell. Note that, from eq. (2.11), a straightforward calculation shows

$$(u_{\vec{0}} - v_{\vec{0}})^2 = \sqrt{\frac{2\omega_J + \omega_A}{\omega_A}}, \tag{5.15}$$

and hence the signal rate is enhanced if $\omega_J \gg \omega_A$.

JHEP08(2021)074

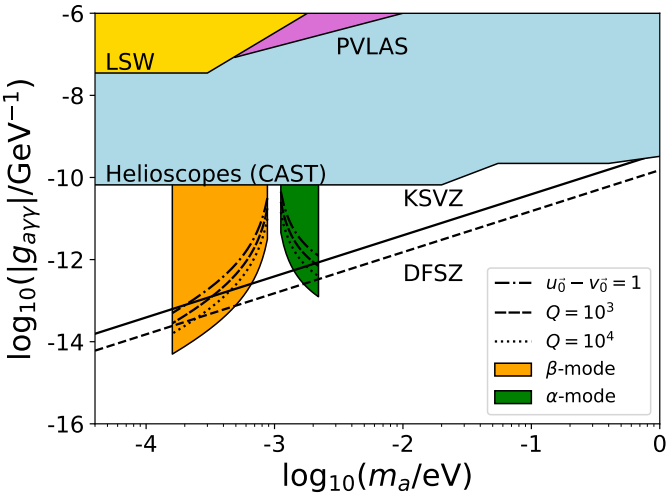

Figure 1. Sensitivity of the magnon to the ALP DM in the m_a vs. $g_{a\gamma\gamma}$ plane. The orange (green) region corresponds to the sensitivity of the β-mode (α-mode) with $u_{\vec{0}} - v_{\vec{0}} = 10$ and $Q = 10^6$, while the dot-dashed, dashed, and dotted lines in each region show the sensitivities of the same setup but with $u_{\vec{0}} - v_{\vec{0}} = 1$, $Q = 10^3$, and $Q = 10^4$, respectively. We postulate the target volume $V = (10\,\mathrm{cm})^3$ and the magnetic field scanned over $1\,\mathrm{T} < B_0 < 7\,\mathrm{T}$ ($1\,\mathrm{T} < B_0 < 10\,\mathrm{T}$) for the β-mode (α-mode). We assume the total observation time $t_{\mathrm{tot}} \sim 1\,\mathrm{yr}$ for the whole scan. See the text for more details of the material properties. Also shown as colored regions are existing constraints, while the black solid (dashed) line shows the prediction for the KSVZ (DFSZ) model.

In figure 1, we show the sensitivity on the ALP parameter space taking $(u_{\vec{0}} - v_{\vec{0}}) = 1$ and 10, $V_{\mathrm{unit}} = (0.3\,\mathrm{keV})^{-3}$, and $|D|^2 = \epsilon = 1$ as the material properties and postulating $V = (10\,\mathrm{cm})^3$. As for the magnon dispersion relation, we use

$$m_m = 1.0 \pm 0.12 \left(\frac{B_0}{1\,\mathrm{T}}\right) \mathrm{meV}, \tag{5.16}$$

where the plus (minus) sign is selected for the α- (β-)mode (see eq. (2.12)). The second term proportional to B_0 corresponds to the Larmor frequency. The reference values of V_{unit}, ω_J and ω_A are taken from those of (Fe-doped) Bi_2Se_3 [39], although it does not correspond to the FKMH model discussed here. We define the quality factor $Q \equiv m_m \tau / 2\pi$ and consider several setups with $Q = 10^3$, 10^4, and 10^6. Note that the last choice corresponds to the most optimistic setup with $\tau_m \gg \tau_a$, in which case the coherence time is estimated as

$$\tau = \tau_a = \frac{2\pi}{m_a v_a^2} \sim 4\,\mu\mathrm{s} \left(\frac{10^{-3}\,\mathrm{eV}}{m_a}\right). \tag{5.17}$$

As a reference value, $Q \sim 300$ is observed for an antiferromagnetic material Rb_2MnF_4 at the temperature $T = 4\,\mathrm{K}$ in [58]. The magnetic field is assumed to be scanned within the range $1\,\mathrm{T} < B_0 < 10\,\mathrm{T}$. The β-mode is used for our analysis only when $B_0 < 7\,\mathrm{T}$ to avoid the instability or the enhanced noise rate according to the low frequency. We assume the total observation time of $t_{\mathrm{tot}} \sim 1\,\mathrm{year}$ for the scan of the whole range of the magnetic field. For a fixed value of the magnetic field, we can search for a mass range of

JHEP08(2021)074

$\Delta m_a \sim 2/\tau \sim 10^{-8}\,\mathrm{eV}$, which combined with $t_{\rm tot}$ allows us to determine the time spent for each scan step. We do not discuss in detail the detection method of generated magnons in this paper; they might be observed through the conversion into photons at the boundary of the material, which are then detected by single photon detectors [59], as demonstrated in ref. [39], or might be detected using some specific features for axionic insulators, such as the dynamical chiral magnetic effect [42]. For the estimation of the sensitivity, we just assume the noise rate for the detection $dN_{\rm noise}/dt \sim 10^{-3}\,\mathrm{s}^{-1}$. We estimate the sensitivity by requiring the signal-to-noise ratio (SNR)

$$(\mathrm{SNR}) \equiv \frac{(dN_{\rm signal}/dt)\,\Delta t_{\rm scan}}{\sqrt{(dN_{\rm noise}/dt)\,\Delta t_{\rm scan}}}, \tag{5.18}$$

to be larger than 3 for each scan step.

In the figure, the orange and green regions correspond to the sensitivity using β- and α-modes, respectively, with $u_{\vec{0}} - v_{\vec{0}} = 10$ and $Q = 10^6$, while the dot-dashed, dashed, and dotted lines in each region show the sensitivities of the same setup but with $u_{\vec{0}} - v_{\vec{0}} = 1$, $Q = 10^3$, and $Q = 10^4$, respectively. The other colored regions show existing constraints from the Light-Shining-through-Walls (LSW) experiments such as the OSQAR [60] (yellow), the measurement of the vacuum magnetic birefringence at the PVLAS [61] (pink), and the observation of the ALP flux from the sun using the helioscope CAST [62] (blue). We also show the predictions of the KSVZ and DFSZ axion models with black solid and dashed lines, respectively. We can see that the use of both α- and β-modes gives a detectability over a broad mass range of 10^{-3}–$10^{-2}\,\mathrm{eV}$ and the sensitivity may reach both the KSVZ and DFSZ model predictions for some mass range. It is also notable that the sensitivity becomes much better for the lighter (heavier) mass region with the β-mode (α-mode), both of which correspond to larger B_0, due to the B_0^4 dependence of the signal rate.

Let us make a comment on the mixing of CM axion to the photon (magnon-polariton). Ref. [39] makes use of the large mixing of them for the DM detection. In our typical values of the parameters, the mixing effect is neglected at the first-order approximation. Actually, the b parameter defined in ref. [39] is given by

$$b \sim 0.006\,\mathrm{meV} \left(\frac{B_0}{2\,\mathrm{T}}\right) \left(\frac{1}{\epsilon}\right)^{1/2} |D|\,(u_{\vec{0}} - v_{\vec{0}}) \left(\frac{m_a}{1\,\mathrm{meV}}\right)^{1/2} \left(\frac{V_{\rm unit}^{1/3}}{(0.3\,\mathrm{keV})^{-1}}\right)^{3/2}. \tag{5.19}$$

Thus we have $b/m_a \ll 1$ for $m_a \sim \mathcal{O}(\mathrm{meV})$ and hence the effective mixing angle is small. Note that the estimate of the mass and decay constant of CM axion in ref. [39] is questionable; see the final paragraph of section 6. This estimation of the effective CM axion-photon mixing is applicable to the case of hidden photon DM discussed in the next subsection with replacing the DM axion mass m_a with the hidden photon mass.

We also comment on the effect of the size of the topological insulator material. In the calculations so far, we have considered a hypothetical infinite size situation, but in the actual experiment it is finite. When a CM axion that has wavelength $\lambda \simeq 2d/n$ (with n being odd integer) is excited in a material with size d, the CM axion reflected at the boundary can additively superimpose the mode before the reflection, forming an amplified

JHEP08(2021)074

stationary wave. The momentum imbalance between DM and CM axion is compensated by the existence of the boundary of the material. In this case, the magnitude of the output signal may be amplified by $\mathcal{O}(10\text{–}100)$ [63], but we do not consider this effect because the size of the amplification strongly depends on the details of the target material, such as size of the mixing between CM axion and photons and reflectance and transmittance of CM axion (or, more precisely, axionic polariton). In particular, the b parameter in our setup is several orders of magnitude smaller than that in [63]. Thus, a detailed analysis is necessary to see how large the amplification due to the size effect can be, which we leave as a future work. The dark matter mass most effectively searched for also differs with d due to the dependence of CM axion momentum on d, but we ignore this effect because the mass difference may be much smaller than the CM axion mass for a reasonable size of material $d \gtrsim \mathcal{O}(1)\,\mathrm{mm}$ [63].

5.2 Hidden photon dark matter

We consider a hidden $U(1)$ gauge field H_μ, which has a kinetic mixing with the $U(1)_Y$ hypercharge gauge boson B_μ. The relevant Lagrangian is

$$\mathcal{L} = -\frac{1}{4}H_{\mu\nu}H^{\mu\nu} - \frac{1}{4}B_{\mu\nu}B^{\mu\nu} + \frac{\epsilon_Y}{2}H_{\mu\nu}B^{\mu\nu} + \frac{1}{2}m_H^2 H_\mu H^\mu, \tag{5.20}$$

where m_H is the hidden photon mass. Below, we use the convention that the expressions such as $H_{\mu\nu}$ and $B_{\mu\nu}$ denote the field strengths of the corresponding gauge fields H_μ and B_μ, respectively. After redefining fields as $B'_\mu \equiv B_\mu - \epsilon_Y H_\mu$ and $H'_\mu \equiv \sqrt{1-\epsilon_Y^2}H_\mu$, we can rewrite the kinetic terms in the canonical form and obtain

$$\mathcal{L} = -\frac{1}{4}H'_{\mu\nu}H'^{\mu\nu} - \frac{1}{4}B'_{\mu\nu}B'^{\mu\nu} + \frac{1}{2}m_{H'}^2 H'_\mu H'^\mu, \tag{5.21}$$

with $m_{H'} \equiv m_H/\sqrt{1-\epsilon_Y^2}$. After the electroweak symmetry breaking, there appear additional mass terms and further mixing occurs. The mass terms are given by

$$\mathcal{L}_{\mathrm{mass}} = \frac{m_Z^2}{2}(c_W W_\mu^3 - s_W B_\mu)^2 + \frac{m_{H'}^2}{2}H'_\mu H'^\mu, \tag{5.22}$$

where m_Z is the Z-boson mass, W_μ^3 is the third component of the $SU(2)_L$ gauge bosons, while $c_W \equiv \cos\theta_W$ and $s_W \equiv \sin\theta_W$ with θ_W being the Weinberg angle. The mass terms are approximately diagonalized by performing the unitary transformation

$$\begin{pmatrix} W_\mu^3 \\ B'_\mu \\ H'_\mu \end{pmatrix} = \begin{pmatrix} c_W & -s_W & s_W c_W \epsilon_Y \\ -s_W & c_W & s_W^2 \epsilon_Y \\ -s_W\epsilon_Y & 0 & 1 \end{pmatrix} \begin{pmatrix} Z_\mu \\ A_\mu \\ H''_\mu \end{pmatrix}, \tag{5.23}$$

up to terms of $O(\epsilon_Y m_H'^2)$ and $O(\epsilon_Y^2 m_Z^2)$. The mass-squared eigenvalues are m_Z^2, 0, and $m_H'^2$ for Z_μ, A_μ, and H''_μ fields, respectively.

According to the mixing among gauge bosons described above, the interaction between H''_μ and electrons is induced as

$$\mathcal{L}_{\mathrm{int}} = -\epsilon_H e H''_\mu \bar{\psi}\gamma^\mu\psi, \tag{5.24}$$

JHEP08(2021)074

where $\epsilon_H \equiv \epsilon_Y c_W$ and ψ is an electron field. Since the electromagnetic interaction of magnons (4.29) originates from the triangle diagram of Dirac electrons, a hidden photon field can replace a photon field in the interaction at the cost of a factor ϵ_H, leading to the magnon-hidden photon-photon interaction

$$H_{\rm int} = -\frac{\epsilon_H \alpha_e}{4\pi}\sqrt{\frac{s}{2N}}(u_{\vec{0}} - v_{\vec{0}})\left[D^*\alpha^\dagger_{\vec{0}} - D\beta^\dagger_{\vec{0}} + \text{h.c.}\right]\int d^3x\, \vec{E}_H \cdot \vec{B}, \tag{5.25}$$

with $\vec{E}_H \equiv -\vec{\nabla}H_0'' - \dot{\vec{H}}''$ being the hidden electric field.

From now on, let us resort to the abbreviation of H_μ and m_H for the mass eigenstate and eigenvalue of the hidden photon for notational simplicity. We consider the light hidden photon to explain the whole amount of the DM.[9] Taking into account the equation of motion $(\Box + m_H^2)H_\mu = 0$ and $\partial_\mu H^\mu = 0$, we can express each component of the hidden photon field as

$$H_0(t,\vec{x}) = -\vec{v}_H \cdot \vec{\tilde{H}}\cos(m_H t - m_H \vec{v}\cdot\vec{x} + \delta), \tag{5.26}$$

$$\vec{H}(t,\vec{x}) = \vec{\tilde{H}}\cos(m_H t - m_H \vec{v}\cdot\vec{x} + \delta), \tag{5.27}$$

with $\rho_{\rm DM} = m_H^2\tilde{H}^2/2$ and $\tilde{H} \equiv |\vec{\tilde{H}}|$. In this parametrization, the hidden electric field is expressed as

$$\vec{E}_H = \vec{\tilde{H}} m_H \sin(m_H t + \delta). \tag{5.28}$$

By repeating the same analysis as in the previous subsection, we can estimate the magnon excitation rate from the existence of the hidden photon coherent oscillation. The rate is given by $dN_{\rm signal}/dt = |C_H|^2\tau/4$ with

$$C_H = -\frac{\alpha_e \tilde{H} m_H B_0 V}{4\pi}\cos\theta\sqrt{\frac{s}{2N}}(u_{\vec{0}} - v_{\vec{0}})D, \tag{5.29}$$

and $\tau = \min(\tau_H, \tau_m)$ with $\tau_H \sim 1/m_H v_H^2$. θ is defined as an angle between $\vec{\tilde{H}}$ and $\vec{B}_0$. Numerically, we obtain the estimation

$$\begin{aligned}\frac{dN_{\rm signal}}{dt} \sim 0.02\,{\rm s}^{-1}&\left(\frac{B_0}{1\,{\rm T}}\right)^2 (u_{\vec{0}} - v_{\vec{0}})^2\left(\frac{V_{\rm unit}}{(0.3\,{\rm keV})^{-3}}\right)\left(\frac{V}{(10\,{\rm cm})^3}\right)\\ &\times|D|^2\left(\frac{\epsilon_H}{10^{-13}}\right)^2\left(\frac{\cos^2\theta}{1/2}\right)\left(\frac{\tau}{0.1\,\mu{\rm s}}\right).\end{aligned} \tag{5.30}$$

Note that the signal rate is proportional to a different power of the magnetic field and the DM mass compared with that for the ALP (5.14).

In figure 2, we show the sensitivity in the hidden photon parameter space. The assumptions for the material properties are the same as those used in the previous subsection, while we assume $\tau \equiv \min(\tau_H, \tau_m)$ with $\tau_H \sim 2\pi/m_H v_H^2$ and $\cos^2\theta = 1/2$ in this case. Again,

[9] The correct relic abundance of hidden photon DM of meV mass range is reasonably explained by the gravitational production mechanism [64–67] or the production from cosmic strings [68]. See also refs. [69–72] for other production mechanisms.

JHEP08(2021)074

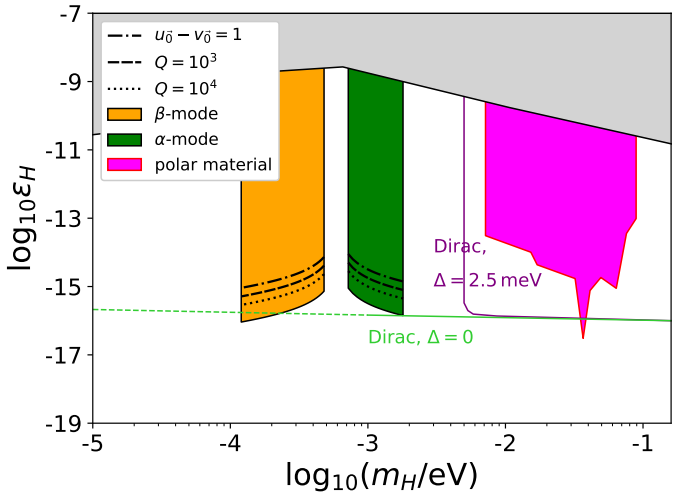

Figure 2. Sensitivity of the magnon to the DM hidden photon in the m_H vs. ϵ plane. The color and line style convention and the experimental set up are the same as those explained in figure 1. The gray region is a combination of existing constraints, while the magenta region shows a sensitivity of the polar material [73]. The purple and green lines correspond to the sensitivity of the Dirac material [74] with gap sizes $\Delta = 2.5\,\mathrm{meV}$ and 0, respectively.

the orange and green regions correspond to the sensitivity of β- and α-modes, respectively. The gray region shows existing constraints taken from [75], while the magenta region shows a sensitivity of the proposal with a polar material [73]. The purple and green lines correspond to the sensitivity of the Dirac material [74] with gap sizes $\Delta = 2.5\,\mathrm{meV}$ and 0, respectively. We can see that the use of magnons gives a good sensitivity over a mass range 10^{-3}–$10^{-2}\,\mathrm{eV}$ of the hidden photon. The sensitivity has a smaller mass dependence compared with the result for the ALP because of the smaller power of B_0 in the expression of the signal rate.

6 Conclusions and discussion

The notion of "axion" appears both in the particle physics and condensed-matter physics. In the particle physics context, the axion is a hypothetical elementary particle introduced to solve the long-standing strong CP problem and it is also one of the good DM candidates. There are lots of efforts to detect axion or axion-like particles, although still it is not discovered yet. Recently there are also increasing interests on the dynamical axion in the condensed-matter context since the developments of theory of topological insulator. Although they share the same name "axion" and have similar electromagnetic properties, their possible relations have been missed except for ref. [39].

Motivated by recent developments in the axion electrodynamics in the context of condensed matter physics, we considered a possibility of DM detection through DM conversion into the condensed-matter (CM) axion. We formulated a way how the CM axion degree of freedom appears starting from the tight-binding model of the electrons on the lattice. In a

JHEP08(2021)074

particular example, we have taken the model in [52], in which the CM axion may be interpreted as the spin wave or the (linear combination of) magnons in an anti-ferromagnetic insulator.[10] For the convenience of readers of particle physics side, we have reviewed the Heisenberg model and half-filling Hubbard model in a self-consistent and comprehensive manner. Based on these basic ingredients, we can derive the CM axion dispersion relation and its interaction with electromagnetic fields.

As DM models, we considered two cases: the elementary particle axion (or ALP) and the hidden photon. We calculated the DM conversion rate into the CM axion in a quantum mechanical way and estimated the signal rate. It is possible to cover the parameter regions which have not been explored so far in the DM mass range of about meV. It may be possible to reach the QCD axion. One should note, however, that our calculation is just based on an idealized theoretical model of the electron system in the anti-ferromagnetic insulator. It is nontrivial how well such a description is when it is applied to a real material. We have not provided a concrete way to detect the CM axion excitation. One possible way is to use the photon emission through the CM axion-photon mixing (axionic polariton) and detect it by the dish antenna as discussed in ref. [39]. It may also be possible to put the material into the cavity and see the cavity photon mode through its mixing with the CM axion, as demonstrated in the context of DM detection with ferromagnetic materials [32, 38]. In any case, it is important to understand the origin of CM axion and its properties, and we believe our formulation gives a basis of the estimation of the CM axion production rate from background DM and is useful for future developments of this field.

The physics of CM axion is very rich and the CM axion in a different material may have a different microphysical origin [42, 43, 76]. It would be interesting to explore the physics of CM axion as a probe of DM in a broader class of materials.

Finally, let us make comments on recent related works that appeared while finalizing this manuscript [63] and after submission of this manuscript [77]. Ref. [63] considered ALP DM detection using the CM axion[11] as an extension of the earlier analysis in ref. [39]. They utilize the material Fe-doped Bi_2Se_3 or $Mn_2Bi_2Te_5$ as an antiferromagnetic insulator and calculated the CM axion mass and decay constant along the line of ref. [41]. Note that ref. [77] pointed out that the concrete numerical values used in the previous calculations including [41] and [63] are not natural and need to be reconsidered. On the other hand, the present paper considers a different realisation of the CM axion from ref. [41]. We first reduce the tight-binding electron model in the Fu-Kane-Mele-Hubbard Hamiltonian to the Heisenberg model and identified the CM axion as a magnon. The calculation of the magnon dispersion relation and its interaction is straightforward. The cost is that the Fu-Kane-Mele-Hubbard model is a toy model and its relation to the real material is not clear at present.

Here we also want to clear up some confusion in the literature. First, the CM axion in the model of Fe-doped Bi_2Se_3 is not described by a linear combination of the magnon,

[10] In the original proposal of dynamical axion in Fe-doped topological insulators such as Bi_2Se_3 [41], the CM axion is interpreted as an amplitude mode of the anti-ferromagnetic order parameter and not expressed by a linear combination of magnons.

[11] The CM axion in this paper is called as "axion quasiparticle (AQ)" in their paper.

JHEP08(2021)074

$\mu \setminus \nu$	s	p_x	p_z	d_{zx}
s	$V_{ss\sigma}$	$n_x V_{sp\sigma}$	$n_z V_{sp\sigma}$	$\sqrt{3} n_x n_z V_{sd\sigma}$
p_x	$*$	$n_x^2 V_{pp\sigma} + (1-n_x^2) V_{pp\pi}$	$n_x n_z V_{pp\sigma} - n_x n_z V_{pp\pi}$	$\sqrt{3} n_x^2 n_z V_{pd\sigma} + n_z(1-2n_x^2) V_{pd\pi}$
p_z	$*$	$*$	$n_z^2 V_{pp\sigma} + (1-n_z^2) V_{pp\pi}$	$n_x V_{pd\pi}$
d_{zx}	$*$	$*$	$*$	$n_x^2 V_{dd\pi} + n_y^2 V_{dd\delta}$

Table 1. Table of off-diagonal elements of $T^{ij}_{\mu\nu}$ [79]. $\vec{n} \equiv \vec{r}_j - \vec{r}_i$ denotes the lattice displacement vector. We omitted the principal quantum numbers associated with μ and ν since a different choice only results in different numerical values of V-factors such as $V_{ss\sigma}$. The left bottom elements with $*$ markers can be obtained by the relationship $T^{ij}_{\mu\nu} = T^{ji}_{\nu\mu} = T^{ij}_{\nu\mu}\big|_{\vec{n}\to-\vec{n}}$.

while it is actually a linear combination in the Fu-Kane-Mele-Hubbard model as shown in this paper. Ref. [39] uses the magnon dispersion relation for the CM axion assuming the Fu-Kane-Mele-Hubbard model, but the authors of ref. [39] incorrectly estimated its decay constant quoting the result of ref. [41] that is only applicable to the Fe-doped Bi_2Se_3 (as mentioned in ref. [63]). They also considered only one of the α- and β-modes. Second, in appendix 1 of ref. [78] (arXiv version) and in section V. A of ref. [42], the CM axion dispersion relation is estimated by the one-loop calculation (or the random phase approximation), but it has been pointed out in ref. [77] that they incorrectly neglected the tree-level contribution to the CM axion mass and also took the wrong sign for the one-loop contribution. Note that appendix 2 of ref. [78] also considered a Heisenberg model limit of the Fu-Kane-Mele-Hubbard model and derived the magnon dispersion relation, which is consistent with our estimation, but its relation to their one-loop calculation is not clear.

Acknowledgments

We thank Koji Ishiwata for useful discussion. This work was supported by JSPS KAKENHI Grant (Nos. 20J00046 [SC], 16H06490 [TM], 18K03608 [TM], 18K03609 [KN] and 17H06359 [KN]). SC was supported by the Director, Office of Science, Office of High Energy Physics of the U.S. Department of Energy under the Contract No. DE-AC02-05CH1123.

A Note on spin-orbit interaction term

In this appendix, we see how to derive the spin-orbit interaction term given in eq. (4.1). We will first discuss how the hamiltonian is expressed in terms of creation and annihilation operators of the electron. Next, we derive the effective hamiltonian of graphene as an example, which becomes the same form as (4.1), and then show that the result is model independent.

A.1 Tight-binding model with spin-orbit interaction

We consider a model in which atoms are attached to lattice points labeled by i with position vectors $\vec{r}_i$. Each atom has its energy eigenstates generated by $c^\dagger_{\mu i}$, where μ denotes an electron orbital. The diagonal part of the tight-binding hamiltonian, $H_{\rm TB}$, is given by the

JHEP08(2021)074

$\mu \setminus \nu$	s	p_x	p_y	p_z
s	0	0	0	0
p_x	0	0	$-is_z$	is_y
p_y	0	is_z	0	$-is_x$
p_z	0	$-is_y$	is_x	0

$\mu \setminus \nu$	d_{xy}	$d_{x^2-y^2}$	d_{zx}	d_{yz}	d_{z^2}
d_{xy}	0	$2is_z$	$-is_x$	is_y	0
$d_{x^2-y^2}$	$-2is_z$	0	is_y	is_x	0
d_{zx}	is_x	$-is_y$	0	$-is_z$	$i\sqrt{3}s_y$
d_{yz}	$-is_y$	$-is_x$	is_z	0	$-i\sqrt{3}s_x$
d_{z^2}	0	0	$-i\sqrt{3}s_y$	$i\sqrt{3}s_x$	0

Table 2. Summary of the matrix elements $\left\langle \vec{L}\cdot\vec{S}\right\rangle_{\mu\nu}$. It is implicitly assumed that the principal quantum numbers of μ and ν are the same. The left (right) panel shows the results for s and p (d) orbitals. Note that the spin operators are related to the Pauli matrices as $s_f = \sigma_f/2$ ($f = x, y, z$).

sum of the hamiltonian of each atom. On the other hand, a small overlap between electron wave functions sit at different lattice sites induces relatively small off-diagonal elements. We are particularly interested in the case where electrons in each atom are tightly bound on a lattice point. In this case, we can neglect the overlap between two sites unless they are the nearest neighbors of each other. Accordingly, we obtain

$$H_{\rm TB} = \sum_{\mu}\sum_{i} \epsilon_\mu c^\dagger_{\mu i} c_{\mu i} + \sum_{\mu,\nu}\sum_{\langle i,j\rangle} T^{ij}_{\mu\nu} c^\dagger_{\mu i} c_{\nu j}, \tag{A.1}$$

where ϵ_μ denotes the energy level of the electron orbital μ of a single atom.[12] The off-diagonal elements $T^{ij}_{\mu\nu}$ are calculated by Slater and Koster [79] as summarized in table 1 for several important choices of electron orbitals. One of the important features of these results is the directional dependence (i.e., the existence of $\vec{n} \equiv \vec{r}_j - \vec{r}_i$ in the expressions), which is sourced from the directional dependence of orbitals. Information of the shape of the lattice comes into the Hamiltonian due to this dependence.

Next, we take into account the effects of the spin-orbit interaction. Due to the relativistic motion of an electron inside an atom, it feels a magnetic field whose size and direction are proportional to its angular momentum $\vec{L}$. As a result, we obtain the on-site spin-orbit interaction Hamiltonian

$$H_{\rm SO} = \frac{1}{m_e^2 r}\frac{dV(r)}{dr}\vec{L}\cdot\vec{S}, \tag{A.2}$$

where $V(r)$ is the centrifugal potential in which the electron moves, while $\vec{L}$ and $\vec{S}$ are the electron angular momentum and spin operators, respectively. Given that the operator $\vec{L}\cdot\vec{S}$ does not change the principal and azimuthal quantum numbers, this interaction induces the term

$$H_{\rm SO} = \sum_{\mu,\nu}\sum_{i} \xi_{n\ell} c^\dagger_{\mu i} \left\langle \vec{L}\cdot\vec{S}\right\rangle_{\mu\nu} c_{\nu i}, \tag{A.3}$$

[12] In general, the energy level may change against the choice of the atom. However, we only focus on the case where it is universal for all the atoms in this paper.

JHEP08(2021)074

where n and ℓ are the common principal and azimuthal quantum numbers of μ and ν, respectively, while $\xi_{n\ell}$ denotes the radial average of the coefficient in eq. (A.2). Some of the matrix elements $\left\langle \vec{L}\cdot\vec{S}\right\rangle_{\mu\nu}$ are shown in table 2 as examples.

A.2 Graphene

Graphene is made of carbon atoms that are located on the two-dimensional honeycomb lattice on the xy plane. Three out of four electrons of the outermost shell of each carbon in $2s$, $2p_x$, and $2p_y$ orbitals are shared among the nearest neighbor carbons to form the so-called σ bond. On the other hand, the other electron in the $2p_z$ orbital is also shared and called the π bond. The unit cell consists of two lattice sites, which we call A and B sublattices. Since we are particularly interested in the dynamics of electrons in p_z orbitals of A and B sublattices, we construct an effective theory of electron states in p_z orbitals by integrating out all the other states.

Among the full hamiltonian $H \equiv H_{\rm TB} + H_{\rm SO}$, we treat the off-diagonal elements, i.e., the second term of eq. (A.1) and $H_{\rm SO}$, as perturbations and name the corresponding part of H as V. Also, we call an effective theory hamiltonian $H_{\rm eff}$ and its off-diagonal part $V_{\rm eff}$, both of which are constructed only from $c_{p_z,i}$ and $c^\dagger_{p_z,i}$. Then, the matching condition of the full theory to the effective theory is given by

$$\left\langle 2p_z, i \left| U^\dagger(t,t_0) \right| 2p_z, j \right\rangle = \left\langle 2p_z, i \left| U^\dagger_{\rm eff}(t,t_0) \right| 2p_z, j \right\rangle , \tag{A.4}$$

where $|\mu, i\rangle \equiv c^\dagger_{\mu i}|0\rangle$ with $|0\rangle$ being the vacuum state, while U and $U_{\rm eff}$ are the time evolution operators in the full and effective theories, respectively. Working in the interaction picture, they are given by

$$U(t,t_0) = T\left\{ \exp\left[i\int_{t_0}^{t} dt'\, V_I(t') \right] \right\}, \tag{A.5}$$

with T being the time-ordering operator, and

$$V_I(t) \equiv e^{iH_0 t} V e^{-iH_0 t}, \tag{A.6}$$

while $U_{\rm eff}$ can be obtained by substituting V with $V_{\rm eff}$.

The left-handed side of eq. (A.4) does not have a contribution from $H_{\rm SO}$ at the first order of V_I since $\vec{L}\cdot\vec{S}$ does not have a non-zero matrix element. Also, there are contributions only with even numbers of $\vec{L}\cdot\vec{S}$ at the second order of perturbation. Such contributions just slightly modify ϵ_μ and $T^{ij}_{\mu\nu}$ and do not qualitatively change the physics, so we just neglect it. The third order contribution can be rewritten as

$$\int_{t_0}^{t} dt' \int_{t'}^{t} dt'' \int_{t''}^{t} dt''' \sum_{\mu,\nu,k,p} \left\langle 2p_z, i \left| iV_I(t') \right| \mu, k \right\rangle \left\langle \mu, k \left| iV_I(t'') \right| \nu, p \right\rangle \left\langle \nu, p \left| iV_I(t''') \right| 2p_z, j \right\rangle . \tag{A.7}$$

According to [80], it is known that the contributions from the spin-orbit interaction among $3d$ orbitals are numerically large in this model, so we may focus only on them. As a result,

JHEP08(2021)074

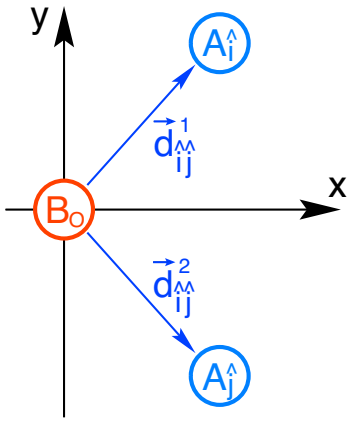

Figure 3. The coordinate adopted in deriving the general form of the spin-orbit interaction.

we deform (A.7) to obtain

$$\left\langle 2p_z, i \left| U^\dagger(t,t_0) \right| 2p_z, j \right\rangle \Big|_{\text{3rd order in } V_I} \simeq -(t-t_0)\frac{\xi_{3d}V_{pd\pi}^2}{(\epsilon_{3d}-\epsilon_{2p})^2}\vec{s}\cdot(\vec{d}^{\,1}_{ij}\times\vec{d}^{\,2}_{ij}), \tag{A.8}$$

where $\vec{d}^{\,1}_{ij} \equiv \vec{r}_k - \vec{r}_i$ and $\vec{d}^{\,2}_{ij} \equiv \vec{r}_j - \vec{r}_k$. The factor $\vec{d}^{\,1}_{ij} \times \vec{d}^{\,2}_{ij}$ forces the matrix element to be zero when $i = j$ and the only non-zero matrix elements are those with (i, j) being a pair of next-nearest neighbors. Therefore, the subscript k in the definition of $\vec{d}_{1,2}$ should be understood as the lattice site in between i and j. The corresponding matrix element in the right-handed side of eq. (A.4) is given by

$$\left\langle 2p_z, i \left| U^\dagger_{\text{eff}}(t,t_0) \right| 2p_z, j \right\rangle \simeq i(t-t_0)\left\langle p_z, i \left| V_{\text{eff}} \right| p_z, j \right\rangle, \tag{A.9}$$

so we conclude

$$V_{\text{eff}} \ni i\frac{\xi_{3d}V_{pd\pi}^2}{(\epsilon_{3d}-\epsilon_{2p})^2}\sum_{\langle\langle i,j\rangle\rangle} c^\dagger_{2p_z,i}\,\vec{s}\cdot(\vec{d}^{\,1}_{ij}\times\vec{d}^{\,2}_{ij})c_{2p_z,j}. \tag{A.10}$$

This agrees with (4.1) when we set $\lambda = a^2\xi_{3d}V_{pd\pi}^2/4(\epsilon_{3d}-\epsilon_{2p})^2$.

A.3 Model independence of the spin-orbit interaction term

So far, we have considered the spin-orbit interaction for a specific choice of the lattice structure, i.e., the two-dimensional honeycomb lattice. Here, we argue that the structure of the interaction, given in eq. (4.1), can be understood by symmetries.

Here, we consider the interaction between next-nearest neighbor sites induced by the spin-orbit interaction H_{SO}. For this purpose, we consider a set of next-nearest neighbor sites from the A-sublattice (called $A_{\hat{i}}$ and $A_{\hat{j}}$), which share only one nearest neighbor site (called B_O). The vectors pointing to $A_{\hat{i}}$ and $A_{\hat{j}}$ from B_O are denoted as $\vec{d}^{\,1}_{\hat{i}\hat{j}}$ and $\vec{d}^{\,2}_{\hat{i}\hat{j}}$, respectively. Here, we adopt a coordinate in which $A_{\hat{i}}$, $A_{\hat{j}}$, and B_O are on the x vs. y plane; the position of B_O is set to be the origin and the y axis is chosen to be parallel to $\vec{d}^{\,1}_{\hat{i}\hat{j}} - \vec{d}^{\,2}_{\hat{i}\hat{j}}$ (see figure 3).

JHEP08(2021)074

Hereafter, we assume that the whole lattice is invariant under the following transformations and hence the Hamiltonian also is:

- $\mathcal{P}$: parity, defined as the reflection with respect to the x vs. y plane: $(x, y, z) \xrightarrow{\mathcal{P}} (x, y, -z)$. With the $\mathcal{P}$ transformation, the angular momentum operator acting on the electron on i-th site transforms as $(L_x^{(i)}, L_y^{(i)}, L_z^{(i)}) \xrightarrow{\mathcal{P}} (-L_x^{(\mathcal{P}[i])}, -L_y^{(\mathcal{P}[i])}, L_z^{(\mathcal{P}[i])})$, where $i \xrightarrow{\mathcal{P}} \mathcal{P}[i]$. (Thus, $\mathcal{P}[\hat{i}] = \hat{i}$.) In addition, the annihilation operator of the electron transforms as

$$c_{\mu,i} \xrightarrow{\mathcal{P}} \sigma_3 c_{\mathcal{P}[\mu],\mathcal{P}[i]}, \tag{A.11}$$

  where $\mathcal{P}[\mu]$ denotes the $\mathcal{P}$-transformed orbital of μ. (If μ is singlet under the $\mathcal{P}$-transformation, $\mathcal{P}[\mu] = \mu$.)

- $\mathcal{R}$: π rotation around the x axis: $(x, y, z) \xrightarrow{\mathcal{R}} (x, -y, -z)$. With this transformation, the lattice site i is moved to the position of $\mathcal{R}[i]$. With $\mathcal{R}$, the angular momentum operator transforms as $(L_x^{(i)}, L_y^{(i)}, L_z^{(i)}) \xrightarrow{\mathcal{R}} (L_x^{\mathcal{R}[j]}, -L_y^{\mathcal{R}[j]}, -L_z^{\mathcal{R}[j]})$. In addition,

$$c_{\mu,i} \xrightarrow{\mathcal{R}} \sigma_1 c_{\mathcal{R}[\mu],\mathcal{R}[i]}, \tag{A.12}$$

  where $\mathcal{R}[\mu]$ denotes the $\mathcal{R}$-transformed orbital of μ.

For example, the diamond lattice used for the Fu-Kane-Mele-Hubbard model and the two-dimensional honeycomb lattice considered in the previous subsection are unchanged under the $\mathcal{P}$ and $\mathcal{R}$ transformations. Then, one can find that the Hubbard model Hamiltonian given in eq. (3.5), tight-binding Hamiltonian given in eq. (A.1), and the spin-orbit interaction given in eq. (A.3) are invariant under the $\mathcal{P}$ and $\mathcal{R}$ transformations.

Starting with the model that is invariant under the $\mathcal{P}$ and $\mathcal{R}$ transformations, the effective theory for the electrons in the orbitals of our interest should also respect these symmetries. In the effective theory, the interaction of the next-nearest neighbor sites can be expressed as

$$H_{\mathrm{NNN}} = \sum_{\langle\langle i,j \rangle\rangle} \left(\ell_{a,ij} c_i^\dagger \sigma_a c_j + t_{ij} c_i^\dagger c_j \right), \tag{A.13}$$

where $\langle\langle i, j\rangle\rangle$ is a set of the next-nearest neighbor sites. (Here, we consider the effective theory containing only the electrons in the unique orbital of our interest, and the index for the electron orbital is omitted for the notational simplicity.)

Now, we discuss the properties of the coefficient $\ell_{a,ij}$ and show that, with $\mathcal{P}$ and $\mathcal{R}$ symmetries, $\vec{\ell}_{ij}$ is proportional to $\vec{d}^1_{ij} \times \vec{d}^2_{ij}$. To see this, we can use the following relations:

$$\ell_{a,\hat{i}\hat{j}} c_{\hat{i}}^\dagger \sigma_a c_{\hat{j}} \xrightarrow{\mathcal{P}} -\ell_{1,\hat{i}\hat{j}} c_{\hat{i}}^\dagger \sigma_1 c_{\hat{j}} - \ell_{2,\hat{i}\hat{j}} c_{\hat{i}}^\dagger \sigma_2 c_{\hat{j}} + \ell_{3,\hat{i}\hat{j}} c_{\hat{i}}^\dagger \sigma_3 c_{\hat{j}}, \tag{A.14}$$

$$\ell_{a,\hat{i}\hat{j}} c_{\hat{i}}^\dagger \sigma_a c_{\hat{j}} \xrightarrow{\mathcal{R}} \ell_{1,\hat{i}\hat{j}} c_{\hat{j}}^\dagger \sigma_1 c_{\hat{i}} - \ell_{2,\hat{i}\hat{j}} c_{\hat{j}}^\dagger \sigma_2 c_{\hat{i}} - \ell_{3,\hat{i}\hat{j}} c_{\hat{j}}^\dagger \sigma_3 c_{\hat{i}}. \tag{A.15}$$

Eq. (A.14) results in $\ell_{1,ij} = \ell_{2,ij} = 0$ while eq. (A.15) implies $\ell_{3,ji} = -\ell_{3,ij}$, and hence we can find that $\vec{\ell}_{ij} \propto \vec{d}^1_{ij} \times \vec{d}^2_{ij}$.

JHEP08(2021)074

	$\widetilde{\alpha}_1$	$\widetilde{\alpha}_2$	$\widetilde{\alpha}_3$	$\widetilde{\alpha}_4$	$\widetilde{\alpha}_5$
U_1	α_5	α_2	α_3	α_4	$-\alpha_1$
U_2	α_1	α_5	α_3	α_4	$-\alpha_2$
U_3	α_1	α_2	α_5	α_4	$-\alpha_3$

Table 3. Transformation law of α-matrices under the unitary transformation by U_1, U_2 and U_3.

B Transformation of $\boldsymbol{\alpha}$ matrix

The chiral representation of α matrices are defined as

$$\alpha_i = \begin{pmatrix} \sigma_i & 0 \\ 0 & -\sigma_i \end{pmatrix}, \quad \alpha_4 = \begin{pmatrix} 0 & -1 \\ -1 & 0 \end{pmatrix}, \quad \alpha_5 = \begin{pmatrix} 0 & -i \\ i & 0 \end{pmatrix}, \tag{B.1}$$

where $\alpha_5 = \alpha_1\alpha_2\alpha_3\alpha_4$. They satisfy the anti-commutation relation $\{\alpha_\mu, \alpha_\nu\} = 2\delta_{\mu\nu}$. Under the unitary transformation $\alpha_\mu \to \widetilde{\alpha}_\mu = U^\dagger \alpha_\mu U$, the anti-commutation relation remains intact. For some choice of U, the α matrices are exchanged. Examples are summarized in table. 3, where

$$U_1 = \frac{1}{\sqrt{2}} \begin{pmatrix} 1 & 0 & 0 & -i \\ 0 & 1 & -i & 0 \\ 0 & -i & 1 & 0 \\ -i & 0 & 0 & 1 \end{pmatrix}, \quad U_2 = \frac{1}{\sqrt{2}} \begin{pmatrix} 1 & 0 & 0 & -1 \\ 0 & 1 & 1 & 0 \\ 0 & -1 & 1 & 0 \\ 1 & 0 & 0 & 1 \end{pmatrix}, \quad U_3 = \frac{1}{\sqrt{2}} \begin{pmatrix} 1 & 0 & -i & 0 \\ 0 & 1 & 0 & i \\ -i & 0 & 1 & 0 \\ 0 & i & 0 & 1 \end{pmatrix}. \tag{B.2}$$

Note that they have the form of

$$U_i = \frac{1}{\sqrt{2}} \begin{pmatrix} 1 & -i\sigma_i \\ -i\sigma_i & 1 \end{pmatrix}. \tag{B.3}$$

for $i = 1, 2, 3$. One can easily show that they yield

$$U_i^\dagger \alpha_j U_i = \begin{cases} \alpha_j & \text{for} \quad i \neq j \\ -\alpha_5 & \text{for} \quad i = j \end{cases}. \tag{B.4}$$

The Dirac representation for the α matrices is given by

$$\alpha_i = \begin{pmatrix} 0 & \sigma_i \\ \sigma_i & 0 \end{pmatrix}, \quad \alpha_4 = \begin{pmatrix} 1 & 0 \\ 0 & -1 \end{pmatrix}, \quad \alpha_5 = \begin{pmatrix} 0 & -i \\ i & 0 \end{pmatrix}, \tag{B.5}$$

The chiral and Dirac representations are related by the unitary transformation as

$$\alpha_\mu^{(\text{Dirac})} = U^\dagger \alpha_\mu^{(\text{chiral})} U, \qquad U = \frac{1}{\sqrt{2}} \begin{pmatrix} 1 & 1 \\ -1 & 1 \end{pmatrix}. \tag{B.6}$$

JHEP08(2021)074

C Berry connection and topological term

C.1 Dimensional reduction of $(4+1)$-dimensional quantum Hall insulator

In section 4, we derived θ using the Lagrangian formulation following ref. [52]. On the other hand, θ can also be expressed in terms of the Berry connection [81, 82].

It is well known that the general $(2+1)$-dimensional quantum Hall insulator is characterized by the first Chern number $N_{\rm ch}^{(1)}$ in terms of the integration of the Berry connection over the Brillouin zone [83]. Its electromagnetic response is described by the action

$$S = \frac{N_{\rm ch}^{(1)}}{4\pi} \int dt d^2x \, \epsilon^{\mu\nu\rho} A_\mu \partial_\nu A_\rho. \tag{C.1}$$

Similarly, the $(4+1)$-dimensional quantum Hall insulator is characterized by the second Chern number $N_{\rm ch}^{(2)}$ and described by the action

$$S = \frac{N_{\rm ch}^{(2)}}{24\pi^2} \int dt d^4x \, \epsilon^{\mu\nu\rho\sigma\tau} A_\mu \partial_\nu A_\rho \partial_\sigma A_\tau, \tag{C.2}$$

where

$$N_{\rm ch}^{(2)} = \frac{1}{32\pi^2} \int_{\rm BZ} d^4k \, \epsilon^{ijkl} {\rm Tr} \left[\mathcal{F}_{ij} \mathcal{F}_{kl} \right], \tag{C.3}$$

with

$$\mathcal{F}_{ij} \equiv \partial_i \mathcal{A}_j - \partial_j \mathcal{A}_i + i[\mathcal{A}_i, \mathcal{A}_j]. \tag{C.4}$$

Here we used a shorthand notation like $\partial_i \equiv \partial/\partial k_i$ and so on (k_4 may be rather understood as $\varphi \equiv k_4 + A_4$) and $\mathcal{A}_i$ denotes the Berry connection matrix in the momentum space given by

$$\mathcal{A}_i^{\alpha\beta} = -i \langle u_k^\alpha | \frac{\partial}{\partial k_i} | u_k^\beta \rangle. \tag{C.5}$$

with $|u_k^\alpha\rangle$ being the Bloch state with α representing the band index, and the trace in eq. (C.4) is taken over the occupied bands. Note that $N_{\rm ch}^{(2)}$ is expressed as

$$N_{\rm ch}^{(2)} = \frac{1}{2\pi} \int \frac{\partial \theta}{\partial \varphi} d\varphi, \tag{C.6}$$

where

$$\theta \equiv \frac{1}{4\pi} \int_{\rm BZ} d^3k \, \epsilon^{ijk} \, {\rm Tr} \left[\mathcal{A}_i \partial_j \mathcal{A}_k + i \frac{2}{3} \mathcal{A}_i \mathcal{A}_j \mathcal{A}_k \right]. \tag{C.7}$$

Now let us perform a dimensional reduction. The action (C.2) is written as

$$S = \frac{1}{8\pi^2} \int dt d^3x \, \epsilon^{\mu\nu\rho\sigma} \frac{\partial \theta}{\partial \varphi} \partial_\mu \varphi A_\nu \partial_\rho A_\sigma = -\frac{1}{8\pi^2} \int dt d^3x \, \theta \, \epsilon^{\mu\nu\rho\sigma} \partial_\mu A_\nu \partial_\rho A_\sigma, \tag{C.8}$$

where we used $\partial_\mu \theta = (\partial\theta/\partial\varphi)\partial_\mu \varphi$. This is an action that describes the electromagnetic response of $(3+1)$-dimensional topological insulator.

JHEP08(2021)074

C.2 Hamiltonian expression of θ

Let us assume the four-band model whose (momentum space) Hamiltonian is given by

$$H = c^\dagger_{k,\alpha}\mathcal{H}_{\alpha\beta}c_{k,\beta}, \qquad \mathcal{H} = \sum_{\mu=1}^{5} R_\mu(\vec{k})\alpha_\mu, \tag{C.9}$$

where $c^\dagger_{k,\alpha}$ and $c_{k,\alpha}$ with $\alpha = 1$–4 denote the electron creation and annihilation operator with the wavenumber k and R_μ are real coefficients. Here we take the Dirac representation for the α matrices (B.5). The Hamiltonian (C.9) is diagonalized by the unitary matrix U:

$$U = \begin{pmatrix} N_+(-R_1+iR_2) & N_+(-R_3+iR_5) & N_-(R_1-iR_2) & N_-(R_3-iR_5) \\ N_+(R_3+iR_5) & N_+(-R_1-iR_2) & N_-(-R_3-iR_5) & N_-(R_1+iR_2) \\ 0 & N_+(R+R_4) & 0 & N_-(R-R_4) \\ N_+(R+R_4) & 0 & N_-(R-R_4) & 0 \end{pmatrix}, \tag{C.10}$$

where $N_\pm \equiv 1/\sqrt{2R(R\pm R_4)}$ and $R \equiv \sqrt{\sum_{\mu=1-5}(R_\mu)^2}$. One finds

$$U^\dagger\mathcal{H}U = \mathrm{diag}(-R,-R,R,R). \tag{C.11}$$

The lower two energy bands and upper two bands are degenerate and we assume that the lower bands are occupied and upper bands are empty. One can define the creation/annihilation operator in the diagonal basis through

$$d_{k,\alpha} \equiv U^\dagger_{\alpha\beta}c_{k,\beta}, \qquad d^\dagger_{k,\alpha} \equiv c^\dagger_{k,\beta}U_{\beta\alpha}. \tag{C.12}$$

The Bloch state may be given by $|u^\alpha_k\rangle = d^\dagger_{k,\alpha}|0\rangle = c^\dagger_{k,\beta}U_{\beta\alpha}|0\rangle$. Thus the Berry connection is calculated as

$$\mathcal{A}_i^{\alpha\beta} = -i\langle 0|U^\dagger_{\alpha\gamma}c_{k,\gamma}\frac{\partial}{\partial k_i}(c^\dagger_{k,\delta}U_{\delta\beta})|0\rangle = -iU^\dagger_{\alpha\gamma}\frac{\partial U_{\gamma\beta}}{\partial k_i}. \tag{C.13}$$

Note that $\mathcal{A}_i^{\alpha\beta}$ is a 2×2 matrix since only the two low energy states are occupied. Substituting the concrete expression (C.10), we obtain

$$\mathcal{A}_i = \sum_{a=1}^{3} A_{ia}\sigma_a, \tag{C.14}$$

where

$$A_{i1} = -N_+^2\left[(R_1\partial_i R_5 - R_5\partial_i R_1) + (R_3\partial_i R_2 - R_2\partial_i R_3)\right], \tag{C.15}$$
$$A_{i2} = -N_+^2\left[(R_3\partial_i R_1 - R_1\partial_i R_3) + (R_5\partial_i R_2 - R_2\partial_i R_5)\right], \tag{C.16}$$
$$A_{i3} = -N_+^2\left[(R_1\partial_i R_2 - R_2\partial_i R_1) + (R_5\partial_i R_3 - R_3\partial_i R_5)\right]. \tag{C.17}$$

Note that the term proportional to the unit matrix $\mathbf{1}$ is canceled.

JHEP08(2021)074

Using the trace formula $\mathrm{Tr}\,[\sigma_a\sigma_b] = 2\delta_{ab}$ and $\mathrm{Tr}\,[\sigma_a\sigma_b\sigma_c] = 2i\epsilon_{abc}$, the first and second terms of θ in (C.7) are calculated as

$$\epsilon^{ijk}\,\mathrm{Tr}\,[\mathcal{A}_i\partial_j\mathcal{A}_k] = \frac{-3}{R^2(R+R_4)^2}\epsilon^{\mu\nu\rho\sigma}R_\mu(\partial_x R_\nu)(\partial_y R_\rho)(\partial_z R_\sigma), \tag{C.18}$$

$$\epsilon^{ijk}\,\mathrm{Tr}\left[i\frac{2}{3}\mathcal{A}_i\mathcal{A}_j\mathcal{A}_k\right] = \frac{R^2-R_4^2}{R^3(R+R_4)^3}\epsilon^{\mu\nu\rho\sigma}R_\mu(\partial_x R_\nu)(\partial_y R_\rho)(\partial_z R_\sigma), \tag{C.19}$$

where $\mu,\nu,\rho,\sigma = 1,2,3,5$. Note that terms proportional $\partial_j N_+$, $\partial_j\partial_k R_\mu$, $\partial_j R_1\partial_k R_1$ and so on vanish when contracted by ϵ^{ijk}. Thus we obtain the following expression for θ,

$$\theta = -\frac{1}{4\pi}\int_{\mathrm{BZ}} d^3k\,\frac{2R+R_4}{R^3(R+R_4)^2}\epsilon^{\mu\nu\rho\sigma}R_\mu(\partial_x R_\nu)(\partial_y R_\rho)(\partial_z R_\sigma). \tag{C.20}$$

This expression is consistent with [76].[13]

References

[1] R.D. Peccei and H.R. Quinn, *CP Conservation in the Presence of Instantons*, *Phys. Rev. Lett.* **38** (1977) 1440 [INSPIRE].

[2] S. Weinberg, *A New Light Boson?*, *Phys. Rev. Lett.* **40** (1978) 223 [INSPIRE].

[3] F. Wilczek, *Problem of Strong P and T Invariance in the Presence of Instantons*, *Phys. Rev. Lett.* **40** (1978) 279 [INSPIRE].

[4] J. Preskill, M.B. Wise and F. Wilczek, *Cosmology of the Invisible Axion*, *Phys. Lett. B* **120** (1983) 127 [INSPIRE].

[5] L.F. Abbott and P. Sikivie, *A Cosmological Bound on the Invisible Axion*, *Phys. Lett. B* **120** (1983) 133 [INSPIRE].

[6] M. Dine and W. Fischler, *The Not So Harmless Axion*, *Phys. Lett. B* **120** (1983) 137 [INSPIRE].

[7] J.E. Kim, *Light Pseudoscalars, Particle Physics and Cosmology*, *Phys. Rept.* **150** (1987) 1 [INSPIRE].

[8] J.E. Kim and G. Carosi, *Axions and the Strong CP Problem*, *Rev. Mod. Phys.* **82** (2010) 557 [*Erratum ibid.* **91** (2019) 049902] [arXiv:0807.3125] [INSPIRE].

[9] M. Kawasaki and K. Nakayama, *Axions: Theory and Cosmological Role*, *Ann. Rev. Nucl. Part. Sci.* **63** (2013) 69 [arXiv:1301.1123] [INSPIRE].

[10] P. Svrček and E. Witten, *Axions In String Theory*, *JHEP* **06** (2006) 051 [hep-th/0605206] [INSPIRE].

[11] A. Arvanitaki, S. Dimopoulos, S. Dubovsky, N. Kaloper and J. March-Russell, *String Axiverse*, *Phys. Rev. D* **81** (2010) 123530 [arXiv:0905.4720] [INSPIRE].

[13] Note that the definition of α_3 and α_5 are reversed between us and ref. [76] and hence there appears an extra minus sign in the final expression (C.20).

JHEP08(2021)074

[12] M. Cicoli, M. Goodsell and A. Ringwald, *The type IIB string axiverse and its low-energy phenomenology*, *JHEP* **10** (2012) 146 [arXiv:1206.0819] [INSPIRE].

[13] P. Sikivie, *Experimental Tests of the Invisible Axion*, *Phys. Rev. Lett.* **51** (1983) 1415 [*Erratum ibid.* **52** (1984) 695] [INSPIRE].

[14] R. Bradley et al., *Microwave cavity searches for dark-matter axions*, *Rev. Mod. Phys.* **75** (2003) 777 [INSPIRE].

[15] ADMX collaboration, *A SQUID-based microwave cavity search for dark-matter axions*, *Phys. Rev. Lett.* **104** (2010) 041301 [arXiv:0910.5914] [INSPIRE].

[16] HAYSTAC collaboration, *Results from phase 1 of the HAYSTAC microwave cavity axion experiment*, *Phys. Rev. D* **97** (2018) 092001 [arXiv:1803.03690] [INSPIRE].

[17] B.T. McAllister, G. Flower, E.N. Ivanov, M. Goryachev, J. Bourhill and M.E. Tobar, *The ORGAN Experiment: An axion haloscope above 15 GHz*, *Phys. Dark Univ.* **18** (2017) 67 [arXiv:1706.00209] [INSPIRE].

[18] D. Alesini, D. Babusci, D. Di Gioacchino, C. Gatti, G. Lamanna and C. Ligi, *The KLASH Proposal*, arXiv:1707.06010 [INSPIRE].

[19] Y.K. Semertzidis et al., *Axion Dark Matter Research with IBS/CAPP*, arXiv:1910.11591 [INSPIRE].

[20] D. Horns, J. Jaeckel, A. Lindner, A. Lobanov, J. Redondo and A. Ringwald, *Searching for WISPy Cold Dark Matter with a Dish Antenna*, *JCAP* **04** (2013) 016 [arXiv:1212.2970] [INSPIRE].

[21] J. Jaeckel and J. Redondo, *Resonant to broadband searches for cold dark matter consisting of weakly interacting slim particles*, *Phys. Rev. D* **88** (2013) 115002 [arXiv:1308.1103] [INSPIRE].

[22] MADMAX Working Group collaboration, *Dielectric Haloscopes: A New Way to Detect Axion Dark Matter*, *Phys. Rev. Lett.* **118** (2017) 091801 [arXiv:1611.05865] [INSPIRE].

[23] Y. Kahn, B.R. Safdi and J. Thaler, *Broadband and Resonant Approaches to Axion Dark Matter Detection*, *Phys. Rev. Lett.* **117** (2016) 141801 [arXiv:1602.01086] [INSPIRE].

[24] I. Obata, T. Fujita and Y. Michimura, *Optical Ring Cavity Search for Axion Dark Matter*, *Phys. Rev. Lett.* **121** (2018) 161301 [arXiv:1805.11753] [INSPIRE].

[25] K. Nagano, T. Fujita, Y. Michimura and I. Obata, *Axion Dark Matter Search with Interferometric Gravitational Wave Detectors*, *Phys. Rev. Lett.* **123** (2019) 111301 [arXiv:1903.02017] [INSPIRE].

[26] M. Lawson, A.J. Millar, M. Pancaldi, E. Vitagliano and F. Wilczek, *Tunable axion plasma haloscopes*, *Phys. Rev. Lett.* **123** (2019) 141802 [arXiv:1904.11872] [INSPIRE].

[27] M. Zarei, S. Shakeri, M. Abdi, D.J.E. Marsh and S. Matarrese, *Probing Virtual Axion-Like Particles by Precision Phase Measurements*, arXiv:1910.09973 [INSPIRE].

[28] D. Budker, P.W. Graham, M. Ledbetter, S. Rajendran and A. Sushkov, *Proposal for a Cosmic Axion Spin Precession Experiment (CASPEr)*, *Phys. Rev. X* **4** (2014) 021030 [arXiv:1306.6089] [INSPIRE].

[29] R. Barbieri, M. Cerdonio, G. Fiorentini and S. Vitale, *Axion to magnon conversion: a scheme for the detection of galactic axions*, *Phys. Lett. B* **226** (1989) 357 [INSPIRE].

JHEP08(2021)074

[30] A.I. Kakhidze and I.V. Kolokolov, *Antiferromagnetic axions detector*, *Sov. Phys. JETP* **72** (1991) 598 [INSPIRE].

[31] P.V. Vorobev, A.I. Kakhidze and I.V. Kolokolov, *Axion wind: A Search for cosmological axion condensate*, *Phys. Atom. Nucl.* **58** (1995) 959 [INSPIRE].

[32] R. Barbieri et al., *Searching for galactic axions through magnetized media: the QUAX proposal*, *Phys. Dark Univ.* **15** (2017) 135 [arXiv:1606.02201] [INSPIRE].

[33] QUAX collaboration, *Axion search with a quantum-limited ferromagnetic haloscope*, *Phys. Rev. Lett.* **124** (2020) 171801 [arXiv:2001.08940] [INSPIRE].

[34] M. Goryachev, B. Mcallister and M.E. Tobar, *Axion detection with precision frequency metrology*, *Phys. Dark Univ.* **26** (2019) 100345 [*Erratum ibid.* **32** (2021) 100787] [arXiv:1806.07141] [INSPIRE].

[35] M.E. Tobar, B.T. McAllister and M. Goryachev, *Modified Axion Electrodynamics as Impressed Electromagnetic Sources Through Oscillating Background Polarization and Magnetization*, *Phys. Dark Univ.* **26** (2019) 100339 [arXiv:1809.01654] [INSPIRE].

[36] M.E. Tobar, B.T. McAllister and M. Goryachev, *Broadband Electrical Action Sensing Techniques with conducting wires for low-mass dark matter axion detection*, *Phys. Dark Univ.* **30** (2020) 100624 [arXiv:2004.06984] [INSPIRE].

[37] M.P. Hertzberg, Y. Li and E.D. Schiappacasse, *Merger of Dark Matter Axion Clumps and Resonant Photon Emission*, *JCAP* **07** (2020) 067 [arXiv:2005.02405] [INSPIRE].

[38] S. Chigusa, T. Moroi and K. Nakayama, *Detecting light boson dark matter through conversion into a magnon*, *Phys. Rev. D* **101** (2020) 096013 [arXiv:2001.10666] [INSPIRE].

[39] D.J.E. Marsh, K.-C. Fong, E.W. Lentz, L. Smejkal and M.N. Ali, *Proposal to Detect Dark Matter using Axionic Topological Antiferromagnets*, *Phys. Rev. Lett.* **123** (2019) 121601 [arXiv:1807.08810] [INSPIRE].

[40] F. Wilczek, *Two Applications of Axion Electrodynamics*, *Phys. Rev. Lett.* **58** (1987) 1799 [INSPIRE].

[41] R. Li, J. Wang, X. Qi and S.-C. Zhang, *Dynamical Axion Field in Topological Magnetic Insulators*, *Nature Phys.* **6** (2010) 284 [arXiv:0908.1537] [INSPIRE].

[42] A. Sekine and K. Nomura, *Axion Electrodynamics in Topological Materials*, *J. Appl. Phys.* **129** (2021) 141101 [arXiv:2011.13601] [INSPIRE].

[43] D.M. Nenno, C.A.C. Garcia, J. Gooth, C. Felser and P. Narang, *Axion physics in condensed-matter systems*, *Nature Rev. Phys.* **2** (2020) 682.

[44] C.L. Kane and E.J. Mele, *Z-2 Topological Order and the Quantum Spin Hall Effect*, *Phys. Rev. Lett.* **95** (2005) 146802 [cond-mat/0506581] [INSPIRE].

[45] L. Fu, C. Kane and E. Mele, *Topological Insulators in Three Dimensions*, *Phys. Rev. Lett.* **98** (2007) 106803 [cond-mat/0607699] [INSPIRE].

[46] L. Fu and C.L. Kane, *Topological insulators with inversion symmetry*, *Physical Review B* **76** (2007) 045302.

[47] M.Z. Hasan and C.L. Kane, *Topological Insulators*, *Rev. Mod. Phys.* **82** (2010) 3045 [arXiv:1002.3895] [INSPIRE].

[48] X.L. Qi and S.C. Zhang, *Topological insulators and superconductors*, *Rev. Mod. Phys.* **83** (2011) 1057 [arXiv:1008.2026] [INSPIRE].

JHEP08(2021)074

[49] A.B. Bernevig and T.L. Hughes, *Topological insulators and topological superconductors*, Princeton University Press, Princeton, NJ, U.S.A. (2013).

[50] C.L. Kane and E.J. Mele, *Quantum Spin Hall Effect in Graphene*, *Phys. Rev. Lett.* **95** (2005) 226801 [cond-mat/0411737] [INSPIRE].

[51] B.A. Bernevig, T.L. Hughes and S.-C. Zhang, *Quantum spin hall effect and topological phase transition in hgte quantum wells*, *Science* **314** (2006) 1757.

[52] A. Sekine and K. Nomura, *Axionic Antiferromagnetic Insulator Phase in a Correlated and Spin–Orbit Coupled System*, *J. Phys. Soc. Jap.* **83** (2014) 104709 [arXiv:1401.4523] [INSPIRE].

[53] C. Kittel, *Theory of antiferromagnetic resonance*, *Phys. Rev.* **82** (1951) 565.

[54] F. Keffer and C. Kittel, *Theory of antiferromagnetic resonance*, *Phys. Rev.* **85** (1952) 329.

[55] J.J. Quinn and K.-S. Yi, *Solid State Physics: Principles and Modern Applications*, Springer, Berlin, Heidelberg (2009), 10.1007/978-3-540-92231-5.

[56] H. Watanabe and H. Murayama, *Unified Description of Nambu-Goldstone Bosons without Lorentz Invariance*, *Phys. Rev. Lett.* **108** (2012) 251602 [arXiv:1203.0609] [INSPIRE].

[57] Y. Hidaka, *Counting rule for Nambu-Goldstone modes in nonrelativistic systems*, *Phys. Rev. Lett.* **110** (2013) 091601 [arXiv:1203.1494] [INSPIRE].

[58] S.P. Bayrakci et al., *Lifetimes of antiferromagnetic magnons in two and three dimensions: Experiment, theory, and numerics*, *Physical Review Letters* **111** (2013) 017204.

[59] S. Komiyama, O. Astafiev, V. Antonov, T. Kutsuwa and H. Hirai, *A single-photon detector in the far-infrared range*, *Nature* **403** (2000) 405.

[60] OSQAR collaboration, *New exclusion limits on scalar and pseudoscalar axionlike particles from light shining through a wall*, *Phys. Rev. D* **92** (2015) 092002 [arXiv:1506.08082] [INSPIRE].

[61] F. Della Valle et al., *The PVLAS experiment: measuring vacuum magnetic birefringence and dichroism with a birefringent Fabry–Perot cavity*, *Eur. Phys. J. C* **76** (2016) 24 [arXiv:1510.08052] [INSPIRE].

[62] CAST collaboration, *New CAST Limit on the Axion-Photon Interaction*, *Nature Phys.* **13** (2017) 584 [arXiv:1705.02290] [INSPIRE].

[63] J. Schütte-Engel et al., *Axion Quasiparticles for Axion Dark Matter Detection*, arXiv:2102.05366 [INSPIRE].

[64] P.W. Graham, J. Mardon and S. Rajendran, *Vector Dark Matter from Inflationary Fluctuations*, *Phys. Rev. D* **93** (2016) 103520 [arXiv:1504.02102] [INSPIRE].

[65] Y. Ema, K. Nakayama and Y. Tang, *Production of purely gravitational dark matter: the case of fermion and vector boson*, *JHEP* **07** (2019) 060 [arXiv:1903.10973] [INSPIRE].

[66] A. Ahmed, B. Grzadkowski and A. Socha, *Gravitational production of vector dark matter*, *JHEP* **08** (2020) 059 [arXiv:2005.01766] [INSPIRE].

[67] E.W. Kolb and A.J. Long, *Completely dark photons from gravitational particle production during the inflationary era*, *JHEP* **03** (2021) 283 [arXiv:2009.03828] [INSPIRE].

[68] A.J. Long and L.-T. Wang, *Dark Photon Dark Matter from a Network of Cosmic Strings*, *Phys. Rev. D* **99** (2019) 063529 [arXiv:1901.03312] [INSPIRE].

JHEP08(2021)074

[69] P. Agrawal, N. Kitajima, M. Reece, T. Sekiguchi and F. Takahashi, *Relic Abundance of Dark Photon Dark Matter*, *Phys. Lett. B* **801** (2020) 135136 [arXiv:1810.07188] [INSPIRE].

[70] J.A. Dror, K. Harigaya and V. Narayan, *Parametric Resonance Production of Ultralight Vector Dark Matter*, *Phys. Rev. D* **99** (2019) 035036 [arXiv:1810.07195] [INSPIRE].

[71] R.T. Co, A. Pierce, Z. Zhang and Y. Zhao, *Dark Photon Dark Matter Produced by Axion Oscillations*, *Phys. Rev. D* **99** (2019) 075002 [arXiv:1810.07196] [INSPIRE].

[72] M. Bastero-Gil, J. Santiago, L. Ubaldi and R. Vega-Morales, *Vector dark matter production at the end of inflation*, *JCAP* **04** (2019) 015 [arXiv:1810.07208] [INSPIRE].

[73] S. Knapen, T. Lin, M. Pyle and K.M. Zurek, *Detection of Light Dark Matter With Optical Phonons in Polar Materials*, *Phys. Lett. B* **785** (2018) 386 [arXiv:1712.06598] [INSPIRE].

[74] Y. Hochberg et al., *Detection of sub-MeV Dark Matter with Three-Dimensional Dirac Materials*, *Phys. Rev. D* **97** (2018) 015004 [arXiv:1708.08929] [INSPIRE].

[75] S.D. McDermott and S.J. Witte, *Cosmological evolution of light dark photon dark matter*, *Phys. Rev. D* **101** (2020) 063030 [arXiv:1911.05086] [INSPIRE].

[76] J. Wang, R. Li, S.-C. Zhang and X.-L. Qi, *Topological magnetic insulators with corundum structure*, *Physical Review Letters* **106** (2011) 126403.

[77] K. Ishiwata, *Axion mass in antiferromagnetic insulators*, *Phys. Rev. D* **104** (2021) 016004 [arXiv:2103.02848] [INSPIRE].

[78] A. Sekine and K. Nomura, *Chiral Magnetic Effect and Anomalous Hall Effect in Antiferromagnetic Insulators with Spin-Orbit Coupling*, *Phys. Rev. Lett.* **116** (2016) 096401 [arXiv:1508.04590] [INSPIRE].

[79] J.C. Slater and G.F. Koster, *Simplified lcao method for the periodic potential problem*, *Phys. Rev.* **94** (1954) 1498.

[80] S. Konschuh, M. Gmitra and J. Fabian, *Tight-binding theory of the spin-orbit coupling in graphene*, *Phys. Rev. B* **82** (2010) 245412.

[81] X.-L. Qi, T. Hughes and S.-C. Zhang, *Topological Field Theory of Time-Reversal Invariant Insulators*, *Phys. Rev. B* **78** (2008) 195424 [arXiv:0802.3537] [INSPIRE].

[82] A.M. Essin, J.E. Moore and D. Vanderbilt, *Magnetoelectric polarizability and axion electrodynamics in crystalline insulators*, *Phys. Rev. Lett.* **102** (2009) 146805 [arXiv:0810.2998] [INSPIRE].

[83] D.J. Thouless, M. Kohmoto, M.P. Nightingale and M. den Nijs, *Quantized Hall Conductance in a Two-Dimensional Periodic Potential*, *Phys. Rev. Lett.* **49** (1982) 405 [INSPIRE].

JHEP08(2021)074